2023

Implementing Super-Resolution of Non-Stationary Tides with Wavelets: An Introduction to CWT_Multi

Matthew Lobo
Princeton University

David A. Jay
Portland State University, djay@pdx.edu

Silvia Innocenti
Environment and Climate Change Canada

Stefan A. Talke
California Polytechnic State University

Steven Dykstra
University of Alaska Fairbanks

See next page for additional authors

Citation Details

Lobo, Matthew; Jay, David A.; Innocenti, Silvia; Talke, Stefan A.; Dykstra, Steven; and Matte, Pascal, "Implementing Super-Resolution of Non-Stationary Tides with Wavelets: An Introduction to CWT_Multi" (2023). [Forthcoming] Journal of Atmospheric and Oceanic Technology https://archives.pdx.edu/ds/psu/40796

Implementing Superresolution of Nonstationary Tides with Wavelets: An Introduction to CWT_Multi

MATTHEW LOBO,[a,b] DAVID A. JAY,[b] SILVIA INNOCENTI,[c] STEFAN A. TALKE,[d] STEVEN L. DYKSTRA,[e,f] AND PASCAL MATTE[c]

[a] *Atmospheric and Oceanic Sciences Program, Princeton University, Princeton, New Jersey*
[b] *Department of Civil and Environmental Engineering, Portland State University, Portland, Oregon*
[c] *Environment and Climate Change Canada, Meteorological Research Division, Québec City, Québec, Canada*
[d] *Civil and Environmental Engineering, California Polytechnic State University, San Luis Obispo, California*
[e] *School of the Earth, Ocean and Environment, University of South Carolina, Columbia, South Carolina*
[f] *College of Fisheries and Ocean Science, University of Alaska Fairbanks, Fairbanks, Alaska*

(Manuscript received 25 October 2023, in final form 29 July 2024, accepted 13 August 2024)

ABSTRACT: Tides are often nonstationary due to nonastronomical influences. Investigating variable tidal properties implies a trade-off between separating adjacent frequencies (using long analysis windows) and resolving their time variations (short analysis windows). Previous continuous wavelet transform (CWT) tidal methods resolved tidal species. Here, we present CWT_Multi, a MATLAB code that 1) uses CWT linearity (via the "response coefficient method") to implement superresolution, i.e., resolving tidal constituents beyond the Rayleigh criterion; 2) provides a Munk–Hasselmann constituent selection criterion appropriate for superresolution; and 3) introduces an objective, time-variable form of inference ("dynamic inference") based on time-varying data properties. CWT_Multi resolves tidal species on time scales of days, and multiple constituents per species with fortnightly filters. It outputs astronomical phase lags and admittances, analyzes multiple records, and provides power spectra of the signal(s), residual(s), and reconstruction(s); confidence limits; and signal-to-noise ratios. Artificial data and water levels from the Lower Columbia River Estuary (LCRE) and San Francisco Bay Delta (SFBD) are used to test CWT_Multi and compare it to harmonic analysis programs NS_Tide and UTide. CWT_Multi provides superior reconstruction, detiding, dynamic analysis utility, and time resolution of constituents (but with broader confidence limits). Dynamic inference resolves closely spaced constituents (like K_1, S_1, and P_1) on fortnightly time scales, quantifying impacts of diel power peaking (with a 24-h period, like S_1) on water levels in the LCRE. CWT_Multi also helps quantify the impacts of high flows and a salt barrier closing on tidal properties in the SFBD. On the other hand, CWT_Multi does not excel at prediction, and results depend on analysis details, as for any method applied to nonstationary data.

SIGNIFICANCE STATEMENT: Ocean tides, especially in coastal and estuarine systems, are often nonstationary, in the sense that the mean and standard deviation of tidal properties vary over time, usually in response to some nontidal process. We introduce here a MATLAB code, CWT_Multi, that uses wavelet transforms to resolve both tidal species and constituents on time scales from a few days to months. Our code accommodates multiple scalar time series and has typical tidal analysis features like constituent selection and inference, plus two forms of uncertainty analyses. It is flexible, allowing the user to adapt analysis properties to diverse datasets. CWT_Multi is applicable to many problems involving time-variable tides, including sea level rise, compound flooding, sediment transport, and wetland habitat analyses. Application to vector data is a straightforward extension, but further development of our uncertainty analysis is merited. Because nonstationary tidal analysis is rapidly advancing, we also define the features of a "well-formed" analysis code.

KEYWORDS: Estuaries; Wavelets; Tides; Rivers; Time series; Spectral analysis/models/distribution

1. Introduction

There are multiple reasons to improve the analysis of time-variable tidal properties. Tides are nonstationary, in the sense that the means and standard deviations of tidal properties vary (cf. Gagniuc 2017), in many environments due to river flow, ocean currents, stratification, and bathymetric change (e.g., reviews by Haigh et al. 2020; Devlin et al. 2018; Talke and Jay 2020), and instrumental errors can introduce specious variations in tidal properties (e.g., Zaron and Jay 2014). Tides and storm surges interact, changing the properties of both (e.g., Horsburgh and Wilson 2007; Familkhalili et al. 2020). Sea level rise (SLR) makes understanding tidal evolution an urgent problem, because changes in tides can either exacerbate or partially ameliorate the effects of SLR (e.g., Devlin et al. 2014; Talke and Jay 2020; Li et al. 2021; Moftakhari et al. 2024). Despite more than 25 years of development of software for nonstationary tides (reviewed by Consoli et al. 2014;

Denotes content that is immediately available upon publication as open access.

Supplemental information related to this paper is available at the Journals Online website: https://doi.org/10.1175/JTECH-D-23-0144.s1.

Corresponding author: David A. Jay, djay@pdx.edu

DOI: 10.1175/JTECH-D-23-0144.1

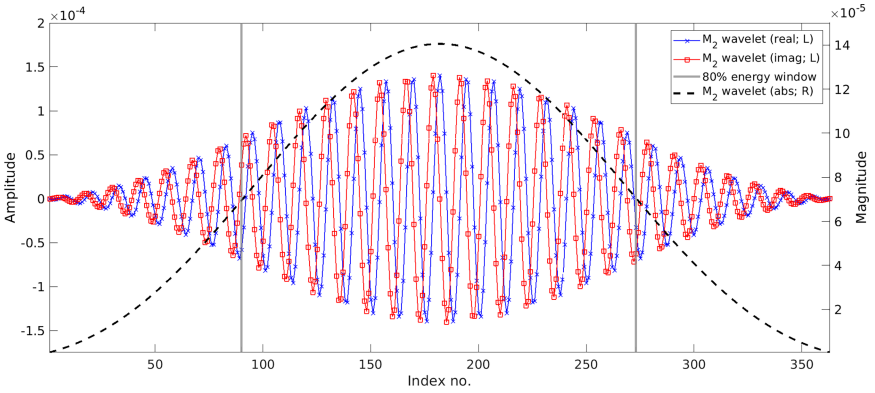

FIG. 1. The real (blue) and imaginary (red) parts of a typical constituent filter as applied to hourly data, in this case for M_2; about 80% of the filter energy is contained in the middle half of the filter (vertical gray lines), as shown by the filter envelope (dotted line). Species filters are shorter, typically 4–8 wavelengths. See Flinchem and Jay (2000) for more information on wavelet filters.

Jay et al. 2022), there is no one approach that is universally applicable, and major challenges still exist in the analysis of tidal signals, often due to the assumptions of the analysis approach (e.g., regarding stationarity and constituent selection) and difficulties with unevenly spaced data and gaps (e.g., Consoli et al. 2014).

Here, we present CWT_Multi, a MATLAB code that uses superresolution (Munk and Hasselmann 1964; henceforth, MH64) to improve continuous wavelet transform (CWT) tidal analysis (Jay and Flinchem 1995, 1997; Flinchem and Jay 2000; Dykstra et al. 2022). Superresolution describes the separation of tidal constituents beyond the conventional Rayleigh criterion limit (Godin 1972), which requires a length of record (LOR) to resolve a frequency difference in LOR^{-1}. This limit is similar to the Heisenberg uncertainty principle of wavelet analysis (Flinchem and Jay 2000). Both quantify the intuition that a short analysis window localizes the time of an event but provides poor frequency resolution, while the opposite is true for a long window. Previous CWT codes (from Jay and Flinchem 1995, 1997 forward) maximized time resolution by analyzing tidal species (e.g., the diurnal or D_1 band and semidiurnal or D_2 band), not constituents within these species. CWT_Multi analyzes tidal species as before, but it also resolves variations of major tidal constituents on a time scale of about a week, choosing constituents using a modified MH64 criterion. Moreover, CWT_Multi provides two forms of uncertainty analysis for tidal parameters: a residual spectrum error analysis similar to Pawlowicz et al. (2002) and Codiga (2011) and a residual resampling approach (Innocenti et al. 2022).

In the methods section, the above innovations are explained, the two systems are analyzed, and then the data used are presented; then, results, discussion, and conclusions sections are presented.

2. Methods

This section describes how CWT_Multi uses multiple filter banks to optimize the time and frequency resolution of nonstationary tides. CWT_Multi resolves large constituents such as M_2, S_2, and N_2 within the D_2 tidal species (and similarly in other species) using fortnightly (~15 days) filters that have most of their energy in the middle half of the filter. Despite the overlapping frequency responses of such filters, closely spaced frequencies can be resolved using the linearity and known frequency response of wavelets (see Jay 1997). In addition, CWT_Multi 1) analyzes and reconstructs multiple, evenly spaced scalar time series; 2) computes power spectra of the input, reconstructed, and residual time series; and 3) introduces dynamic inference, a form of tidal inference that uses the properties of the subject time series to separate closely spaced frequencies. Implementation details for CWT_Multi, UTide, and NS_Tide are provided in the online supplemental material.

a. Overview

CWT_Multi convolves four different filter banks with a high-passed version of a water-level time series at each analysis time step; the high-pass filter removes the subtidal component of the signal. In each filter bank, each filter's central frequency corresponds to a tidal species or a tidal constituent within the D_1–D_4 species (Fig. 1). Tidal frequencies are closely spaced (e.g., Fig. S1b in the supplemental material), and the finite length of each filter causes it to respond to signal energy at other tidal frequencies close to its central frequency, as shown in a filter frequency response plot (Fig. 2). Using the linearity and known response function of wavelet filters (Kaiser 2011), a matrix problem is constructed [the response coefficient method (RCM)] to estimate the amplitude of the constituent at the fundamental frequency, effectively removing the filter's response at nearby frequencies, described below. A conceptual view of the use of the four filter banks is provided in Fig. 3.

The species filter bank contains the shortest filters and provides the finest time resolution of varying tidal properties (Fig. 3). A length of about six wavelengths is chosen for the

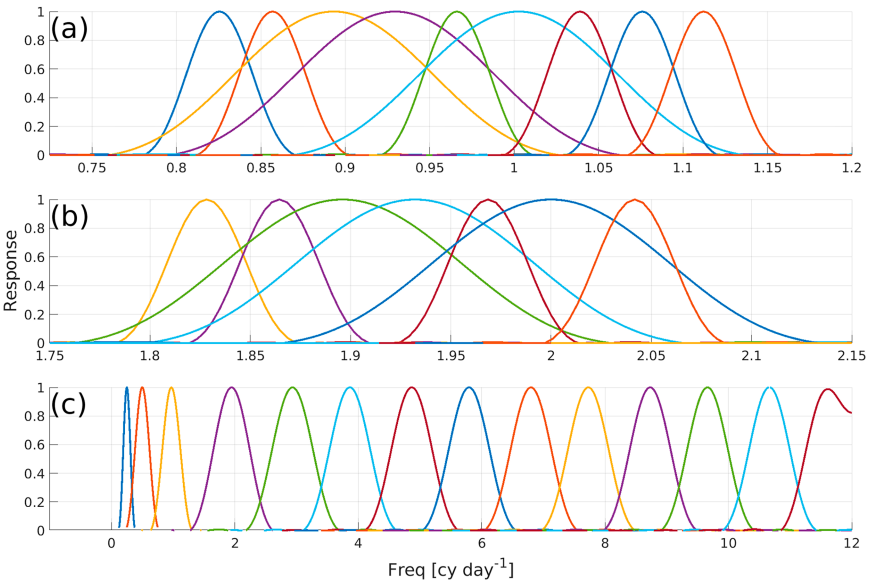

FIG. 2. Frequency response of the default filter banks: (a) D_1 filters, (from left to right) Alp_1, $2Q_1$, and Q_1 (15 days); O_1 (15 days); NO_1 and K_1 (15 days); and J_1, OO_1, and Ups_1; (b) D_2 filters, (from left to right) Eps_2, Mu_2, and N_2 (15 days); M_2 (15 days); L_2 and S_2 (15 days); and Eta_2; and (c) species filters, (from left to right) D_1–D_{12}. Filters are normalized to provide unit response at their central frequency to unit input at that frequency. Short filters have a wider response function than narrow filters; see Table S1 for filter properties.

D_1 and D_2 species, reducing filter overlap between tidal species to a tractable level. A length of 65 h is used for the D_3 and higher frequencies to efficiently capture tidal variance, while still limiting species overlap. This filter bank is similar to that used by Jay and Flinchem (1997), but its use is modified here to remove the effects of leakage between filters.

Tidal constituents within a tidal species may respond differently to external forcing, e.g., to river flow fluctuations (e.g., Jay and Flinchem 1997; Godin 1999). Thus, a second filter set, the "fortnightly filters," is used to resolve the three major components within the diurnal and semidiurnal constituent groups (Fig. 3). These filters are 15 days long and resolve by default the Q_1, O_1, and K_1 constituent groups in the D_1 species and the N_2, M_2, and S_2 groups in the D_2 species; they are long enough to have near-zero frequency response outside of their tidal species. By a "constituent group," we mean constituents that share the first two Doodson numbers, as defined by Cartwright and Edden (1973). Thus, constituent K_1, with the modified Doodson numbers {1, 1, 0, 0, 0, 0}, is represented here as {1, 1, 0}, while the K_1 constituent group, containing K_1, P_1, S_1, and other smaller constituents, is denoted by {1, 1, n}, which indicates that all constituents in the group have a frequency that is the sum of 1 cycle per day + 1 cycle per month + n cycles per year, with n being a small integer, $-5 < n < 5$. In practice, frequency differences within major constituent groups are 1–4 cycles per year.

There is an overlap in the response of adjacent fortnightly filters; thus, the O_1 filter responds to Q_1 and K_1, the Q_1 filter responds to O_1 and K_1, and so on. However, the linearity of wavelet filters and their known frequency response allows us to disentangle the filter responses of the constituent groups in the D_1–D_4 species. "Linearity" means that a CWT filter's response to two signals is the sum of its responses to the signals individually (Rioul and Vetterli 1991), and the frequency response of a CWT filter is known from the Fourier transform of the filter (Kaiser 2011). These major constituent group estimates are, however, contaminated by filter response to other nearby, smaller constituent groups.

This cross talk between constituent groups suggests the use of additional filters for other constituent groups. Unfortunately, attempting to resolve the constituent groups customarily used in harmonic analysis (HA), nine (from {1, −4, n} to {1, 4, n}) in the D_1 band and seven in the D_2 band (from {2, −3, n} to {2, 3, n}), can result in unstable matrix inversions with 15-day filters. This problem is avoided by introducing a third set of filters, with lengths of ~45 days for the "smaller" D_1 and D_2 constituent groups, i.e., the six D_1 and four D_2 groups not named above (Fig. 3). Given filter outputs for nine D_1 constituent groups and seven D_2 groups, estimates of all constituent groups in each species are derived. Like constituent estimates obtained by HA with similar window lengths, each constituent group estimate is influenced by all the constituents within the group. Such estimates are, therefore, time variable, even if the signal analyzed is relatively stationary.

Optionally, a fourth set of wavelet filters of length 4383 h (~182 days) is used in coordination with the fortnightly filters to separate large constituents within the same constituent group, in particular K_1 and P_1 in the K_1 group and S_2 and K_2 in the S_2 group (Fig. 3). Within each of these constituent pairs, the constituents are separated by 2 cycles per year. These "half-yearly" filters provide continuous estimates of the complex

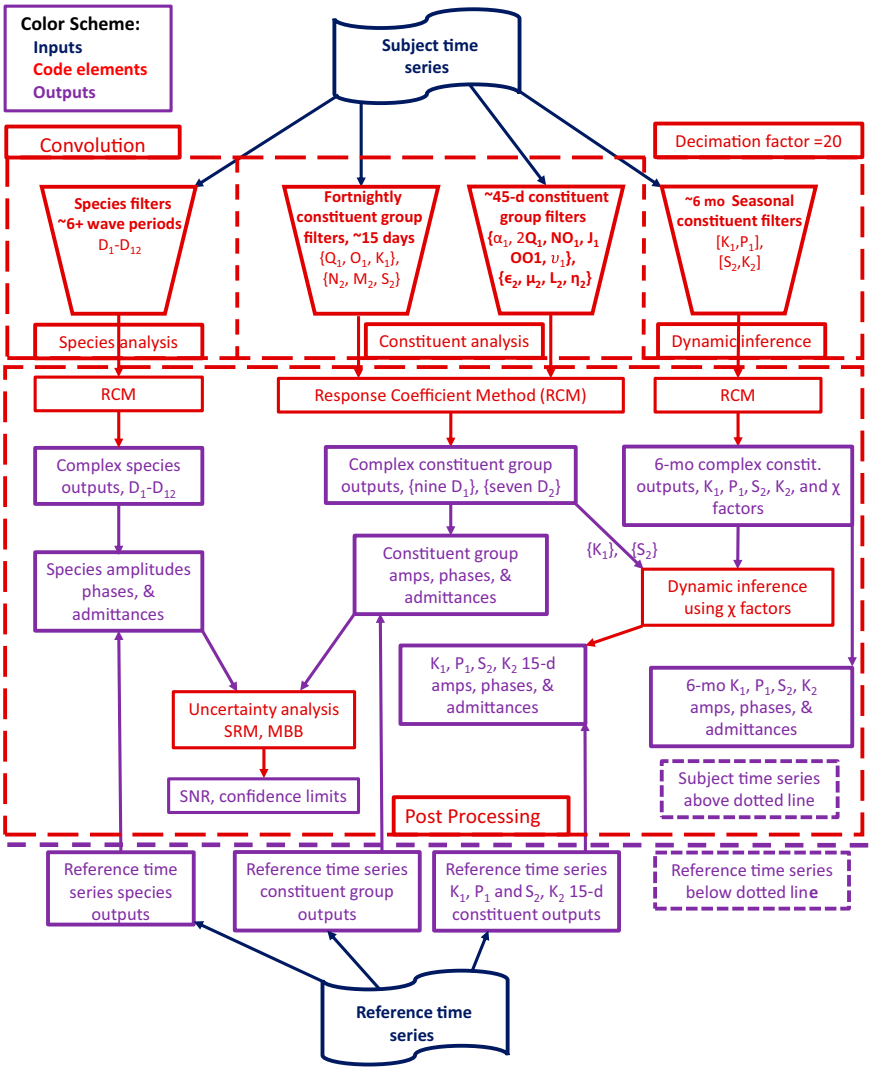

FIG. 3. A conceptual view of the default CWT_Multi analysis process. Input signals are in dark blue, code elements are in red, and outputs are in purple. The analysis for a scalar "Subject Time Series" is shown in detail; only outputs are shown for the "Reference Time Series," which is normally chosen as the local astronomical tidal potential or a nearby coastal station. Constituent groups within a tidal species are shown as, for example, $\{Q_1, O_1, K_1\}$; constituents in a constituent group are shown as $[K_1, P_1]$. SRM = spectral residual method; MBB = moving block bootstrap method. Note that the "species analysis," "constituent analysis," and dynamic inference involve different filters and convolutions, but the latter two interact during "postprocessing."

ratios of the relevant constituents that are used with the fortnightly filter outputs to provide fortnightly scale estimates of K_1 and P_1 and S_2 and K_2 using dynamic inference (below).

b. *Wavelet properties and convolution*

We follow Flinchem and Jay (2000) in building CWT filter banks (Fig. 1) from Kaiser filters tuned to known tidal frequencies (from Cartwright and Edden 1973). Because the filters have real and imaginary parts, the convolution of each filter with the subject time series returns real and imaginary parts that can be resolved into estimates of the amplitude and phase at each convolution time. Kaiser filters (Kaiser 2011) are used, because they minimize the amplitude of the first side lobe of the filter, but Morlet (Gaussian) filters would yield similar results. As described in Flinchem and Jay (2000), wavelet convolution applies each filter window to the product of the signal and associated weights (1 for data present and 0 for missing data), translating the filter from beginning to end of the signal by a decimation factor (20 h by default). Filter lengths of 6–8 wave periods are appropriate for tidal species. A filter length of 15 days (the fortnightly filters) facilitates the resolution of major tidal constituent groups. Filters with default length of 45 and 183 days are used to facilitate the separation of smaller constituent groups and closely spaced

constituents. Due to the tapered nature of the wavelet filters, >80% of the signal's energy is captured by the middle 50% of the wavelet filter (Fig. 2). Finally, because wavelet filters are symmetric (real part) or antisymmetric (imaginary part) in time, they are "phase linear"; i.e., phase information is not distorted. For all filters, gappy data are accommodated using weights in the convolution operation—missing data are given a weight of zero, and windows with more than 10% missing data return a not a number (NaN).

c. *Species solution*

The first section of the analysis code estimates amplitudes and phases of the major tidal species and reconstructs the input data. The species filters are short and have a broad frequency response (relative to the constituent filters used below) to maximize their responses to the collection of constituents within each tidal species (Fig. 2). They optimize the capture of temporal variability, e.g., as occurs during a short, river flow event, and are very useful for detiding nonstationary data. The primary difference between the CWT_Multi species approach and earlier CWT analyses is that the RCM is used to remove any overlap between adjacent species (below). The CWT_Multi package provides a default species filter bank with one filter per tidal species, from once to 12 times daily (i.e., D_1–D_{12}; Table S1a).

d. *Linearity and the RCM*

One challenge in separating constituent groups within a tidal species like D_1 is that the response functions of their filters overlap (Fig. 2). Another is that there is a continuum of nontidal energy that coexists with the tidal signal. The magnitude of that energy determines whether constituents estimated by CWT_Multi (or any tidal code) are meaningful, because tidal estimates inevitably include nontidal background energy as well. However, wavelet convolution is a linear operation, and wavelet filters have a known response function, allowing the elimination of filter overlap. Thus, the RCM assumes that tidal energy exists as separate bands and that energy outside of these bands is small. We illustrate the separation of the three largest D_1 constituent groups, Q_1, O_1, and K_1, with fortnightly filters (the wide filters in Fig. 2a), as a simplified example. Thus, we construct a response coefficient matrix $\mathbf{R}$ as follows:

$$\mathbf{R} = \begin{bmatrix} r_{1,1} & r_{1,2} & r_{1,3} \\ r_{2,1} & r_{2,2} & r_{2,3} \\ r_{3,1} & r_{3,2} & r_{3,3} \end{bmatrix}, \tag{1}$$

where $r_{i,j}$ is the response of the filter with tidal frequency i to a signal of unit amplitude at frequency j; constituent groups are ordered by frequency within a species; hence, $r_{1,2}$ is the response of the Q_1 filter to a unit O_1 signal, which can also be written as $r_{Q1,O1}$. Using $\mathbf{R}$, we create a linear system of equations:

$$\mathbf{f}(t_m) = \mathbf{R}\,\mathbf{a}(t_m), \tag{2}$$

where $\mathbf{f}(t_m) = [A'_{Q1}(t_m), A'_{O1}(t_m), A'_{K1}(t_m)]$ is a column vector of the complex response of each filter to the signal, as applied at time t_m, with $m = 1, 2, \ldots, n$, where n is the number of estimates for each group resulting from the convolution process; $\mathbf{a}(t_m) = [A_{Q1}(t_m), A_{O1}(t_m), A_{K1}(t_m)]$ is a column vector of the estimated complex values for the three constituent groups at a given time; and primed variables are raw output that contains information from multiple constituents. The RCM consists of inverting Eq. (2) to obtain estimates of the constituent group properties $\mathbf{a}(t_m)$ with the cross talk between filters eliminated. Because $\mathbf{R}$ is a function solely of filter lengths and frequencies, it only needs to be determined once; $r_{i,j} = r_{j,i}$, so long as filters i and j are the same length. In practice, the D_1 constituent group solution uses all nine filters shown in Fig. 2a, as explained in the next section, and $\mathbf{R}$ loses its symmetry. A numerical example of the matrix inversion implied by Eq. (2) is supplied in the supplemental material, section 1.1.

The RCM enhances the power of a CWT tidal analysis, because it facilitates time–frequency resolution of tidal properties beyond the limits implied by the Heisenberg principle. By default, CWT_Multi uses fortnightly filters for three constituents per species for D_1 and D_2; the number of filters and filter lengths are user adjustable.

e. *Constituent solution—Combining fortnightly and 45-day filters*

CWT_Multi uses fortnightly and 45-day filters to separate constituent groups within tidal species (Table S1b). Constituent groups are separated by ±1 cycle per month, and there is one filter per constituent group for D_1 groups from $\{1, -4, n\}$ to $\{1, 4, n\}$ and for D_2 groups from $\{2, -3, n\}$ to $\{2, 3, n\}$, yielding nine and seven output time series, respectively. By default, fortnightly filters are used for the N_2, M_2, and S_2 groups and Q_1, O_1, and K_1 groups, to track their evolution on short time scales. Longer (45 days) filters are used for smaller constituent groups, to remove their influence on the major constituents. The RCM is applied separately within each tidal species (D_1–D_4), because the overlap between filters in different species is very small. The default filter lengths are adjustable but not arbitrary—experience shows that filters shorter than 15 days do not greatly increase time resolution but yield noisier outputs, because the shorter filters have a broader frequency response. For the terdiurnal (D_3) and quarter diurnal (D_4) overtides, there are four frequencies each, with most filters set to a length of 45 days to ensure a fairly narrow frequency response; filters for MK_3 and M_4 are, however, fortnightly. Higher overtide frequency filters (one per species, D_5–D_{12}) are set to 65 h, allowing for a broad response and rapid program execution (Table S1b). If a specific high overtide were of interest, longer filters could be used. The RCM is not used for species D_5–D_{12}.

f. *Tidal admittances*

Tidal admittance Γ_A is the complex ratio of a constituent or species estimated from data to the same quantity in the astronomical tidal potential η used as a reference (Munk and Cartwright 1966). While η contains frequencies from subtidal up through D_3, the D_3 signal in many tidal records stems

mainly from nonlinear generation, as do all higher overtides. Simon (1991) introduced, therefore, the use of a nearby coastal station with relatively stationary data as a reference, a quantity we call Γ_C. Simon used Γ_C for river tide prediction, but the use of Γ_C also reduces interference from constituents not analyzed (because their effects are similar in the signal of interest and the reference), facilitating dynamical analyses (Jay and Flinchem 1997). The term Γ_A and/or Γ_C may be optionally estimated by CWT_Multi; we use η as calculated by a NASA routine (R. Ray 2007, personal communication).

g. Dynamic inference

Traditional tidal inference employs user-defined complex ratios between major and minor constituents to separate constituents that cannot be directly resolved, given the analysis window length. CWT_Multi deduces constituent ratios from the output of seasonal (183 days) filters (Table S1c); these allow resolution on a fortnightly scale of constituents separated by 1–4 cycles per year within a constituent group, a process we call dynamic inference. For example, a set of seasonal filters can be used to resolve the "base frequency" K_1 of the K_1 group and one or more "auxiliary" constituents, like P_1.

To explain dynamic inference, we introduce the concept of the group (complex) amplitude A_G. For fortnightly filters distinguished by an accent (˜) $\tilde{A}_G(t)$ is the filter response at the base frequency after the removal of interference from other groups. In the K_1 group, for example, $\tilde{A}_G(t) \equiv \tilde{A}_{K1}(t)$, because the fortnightly K_1 filter responds to all constituents in the constituent group.

For seasonal filters, distinguished by the overbar (¯), we define complex group amplitude:

$$\overline{A}_G(t) \equiv \sum_{j=1}^{n} \overline{A}_j(t), \tag{3a}$$

where the $\overline{A}_j$, for $j = 1, \ldots, n$ seasonal filter outputs for the base constituent plus one or more auxiliary constituents, after removal of filter overlap. For $\overline{A}_G$, it is typically best to capture all frequencies that are separable at the seasonal level, even though not all are significant at the fortnightly level. Thus, n may be larger than 2. For example, there may be considerable, irregular nonastronomical forcing at S_1 (period 24 h) that affects estimates of K_1 and P_1. In such a case, using three filters at the seasonal level (K_1, P_1, and S_1) may be useful for removing the contamination at the fortnightly scale of K_1 by S_1, even if S_1 is not individually meaningful at that scale. While the Rayleigh criterion suggests that a 4383-h analysis cannot resolve these three constituents separated by 1 cycle per year, this is usually possible using the RCM, given sufficient energy in S_1 and limited nonstationarity. We then define $j = 1, n$ complex constituent ratios:

$$\overline{\chi}_j(t) = \frac{\overline{A}_j(t)}{\overline{A}_G(t)}, \tag{3b}$$

with $\overline{\chi}_1$ being the base frequency ratio. Then, the values of the base and auxiliary constituent on the fortnightly time scale are

$$\tilde{A}_{k,\mathrm{inf}}(t) = \tilde{A}_G \frac{\overline{\chi}_k(t)}{r_{\mathrm{group},k}}, \; k = 1, 2, \tag{4}$$

where subscript inf implies a dynamically inferred complex response, $r_{\mathrm{group},k}$ is the response of the kth constituent to the base frequency, and $r_{\mathrm{group,base}} = 1$.

By default, CWT_Multi uses dynamic inference to provide fortnightly estimates of K_1 and P_1, and S_2 and K_2. These values are supplemental to the K_1 and S_2 estimates discussed above. At some cost in computation time, dynamic inference can be applied in additional constituent groups (e.g., to separate N_2 and Nu_2 in the N_2 group) or to determine more than two constituents in the K_1 and/or S_2 constituent groups.

Dynamic inference improves on the usual inference approach used in HA, because the inference is objective (determined by the time series) and not imposed by the user; in this respect, it resembles the inference approach of Pan et al. (2023b), though unlike Pan et al. there is no dependence on the "credo of smoothness" of Munk and Cartwright (1966), so inference can be used with constituents like S_1, where nonastronomical influences are often strong. Also, $\overline{\chi}_j(t)$ varies over the length of a time series, depending on the data. Still, two issues limit the utility of the dynamic inference method:

- Small constituents in a constituent group that are not resolved at the seasonal scale may contaminate estimates of resolved constituents, just as in a HA with inference.
- The complex frequency ratios within a constituent group should change slowly (i.e., seasonally), even if constituent group properties vary more rapidly. This is the temporal analog of the Munk and Cartwright (1966) spectral credo of smoothness. Its adequacy is a question of the physics causing the nonstationary behavior.

Adjustment of filter lengths and/or frequencies analyzed may be needed to minimize these issues. Alternatively, the inferred values can be ignored in favor of constituent group results.

h. Constituent selection

The linearity and known response functions of wavelet filters simplify the constituent selection problem relative to least squares HA, because the response to any single CWT filter is independent of whether other filters are included in the analysis. Thus, constituent selection can be conducted postanalysis. Also, it is usually desirable to remove filter overlap using the RCM, regardless of whether all constituents (or species) rise above the noise floor. We begin from the MH64 criterion for the minimum frequency separation of tidal constituents Δf adapted to the wavelet filters:

$$\Delta f > \frac{1}{\frac{1}{2}\mathrm{LOF} \times \mathrm{SNR}}, \tag{5a}$$

where LOF is the filter length and SNR is the signal-to-noise ratio for a constituent. The factor (1/2)LOF is used instead of LOF because most filter energy is in the middle half of the filter (Fig. 1). Following the meteorological literature

(e.g., Deser et al. 2014), we define SNR as a ratio of quantities with units of length:

$$\mathrm{SNR} = \frac{\mathrm{Amp}}{\text{standard error}}. \tag{5b}$$

In this form, an SNR ≥ 2 indicates that a constituent is above the noise floor by an amount equivalent to its 95% confidence limit. Because MH64 defines SNR as the square of our SNR, we use SNR in Eq. (5b), not $\mathrm{SNR}^{1/2}$. Moreover, Eq. (5a) is appropriate for the species analysis but does not take into account the improvement of resolution through the RCM. For constituent analysis, we modify Eq. (5a) for each constituent i:

$$\frac{\Delta f_i}{C_R} > \frac{1}{\frac{1}{2}\mathrm{LOF} \times \mathrm{SNR}} \times \left\{1 - \frac{r_{ii}|A_i|}{\mathrm{Sqrt}\left[\sum_{j=1}^{n}\left(r_{ij}|A_{ij}|\right)^2\right]}\right\}, \tag{5c}$$

where $|A_i|$ is the time average of the complex amplitude of the ith constituent, C_R is an $O(1)$, user-chosen Rayleigh constant, and the summation is over the n constituents analyzed within a species; $r_{i,i} = 1$. Equation (5c), while heuristic, emphasizes that the RCM improves the resolution of the larger constituents more than that of the smaller ones, closer to the noise floor. The outputs from Eqs. (5a) and (5c) indicate whether a species or constituent is distinct, while confidence limits provide an assessment of uncertainty.

i. Uncertainty analysis

Two different methods are used to estimate the standard errors of the nonstationary outputs: a spectral residual method (SRM) that calculates the parameter standard errors from the residual energy following Pawlowicz et al. (2002); and a moving block bootstrap (MBB) method based on residual resampling. Both methods are thoroughly discussed in Innocenti et al. (2022). MBB divides the residual time series into 30-day blocks, and then, the segments are randomized and added back to the reconstruction of the original signal, for both the species and constituent methods. Next, these new time series are analyzed and reconstructed. This process is repeated n_r times to generate n_r independent estimates of each nonstationary amplitude. These estimates are converted to standard errors and confidence intervals; $n_r = 1000$ in Innocenti et al. (2022).

3. Background, setting, and data

Tides respond to river flow in the Lower Columbia River Estuary (LCRE) and San Francisco Bay Delta (SFBD) in a consistent manner (Jay and Kukulka 2003; Baranes et al. 2023), and this response can be used to hindcast river inflow (Moftakhari et al. 2013, 2015, 2016; Talke et al. 2020). Accordingly, these systems are useful for testing tidal analysis software. Here, we describe the LCRE and SFBD tidal systems, the data used from each system, artificial data used to test CWT_Multi, and development of nonstationary tidal methods over the last few decades.

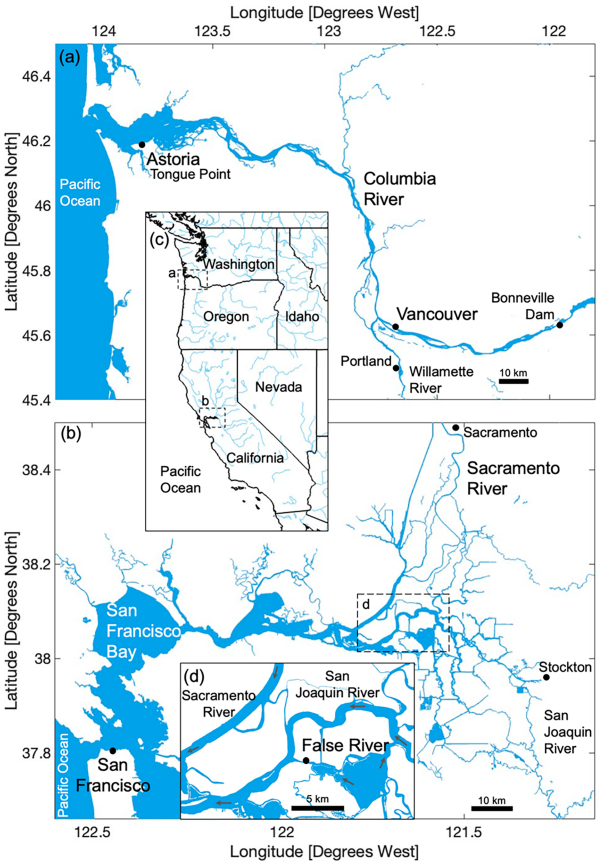

FIG. 4. Place-name maps for (a) the LCRE and (b) the SFBD; their locations are shown in insets (c) and (d), respectively.

a. The LCRE

The LCRE (Figs. 4a,c) extends 233 km from the Pacific to the head of the tide at Bonneville Dam. Regulated river inflow ranges from 1800 to 26 000 $\mathrm{m^3\ s^{-1}}$ (Jay and Naik 2011; Naik and Jay 2011). The LCRE is strongly tidal for about 170 km, from the ocean to the end of the navigation channel. Further landward, tides are weak or absent, except during low-flow periods (Jay et al. 2014, 2016). Tides entering the system are mixed D_1 and D_2, but D_2 dominant (Jay 1984; Jay and Smith 1990). Thus, the M_2 and K_1 amplitudes at the National Oceanic and Atmospheric Administration (NOAA) reference tidal station [Tongue Point, river kilometer (Rkm)-29] are, respectively, $|M_2| = 0.98$ m and $|K_1| = 0.41$ m. Hydropower peaking at Bonneville Dam causes the water-level power spectrum to exhibit pronounced diel (at the frequency of S_1) and weekly variability as far seaward as Rkm-87. The form factor $(|M_2| + |S_2| + |N_2|)/(|K_1| + |O_1| + |P_1|)$ is about 1.7 at Astoria but varies along the channel due to power peaking, constituent interactions, and frequency-variable damping (Jay et al. 2014).

Amplitudes of major D_1 and D_2 tidal constituents have grown 5%–7% at Tongue Point since 1925, one of the fastest increases in the eastern Pacific (Jay 2009; Talke et al. 2020). This increase is largely due to decreased friction, caused by

reduced mean flow and navigational development (Jay et al. 2011, 2014; Helaire et al. 2019, 2020). Interestingly, SLR has not been a major factor in increasing tidal amplitudes, because relative SLR has been only 0.06 ± 0.04 m since 1853 (Talke et al. 2020), and water levels in the tidal river have actually dropped, due to decreased friction (Jay et al. 2011). High river flow strongly damps tides (time scales of days to months), and neap-spring changes in friction alter tidal and subtidal water-level patterns (Jay and Flinchem 1997; Kukulka and Jay 2003a,b).

Hourly water-level data from April 2010 to June 2013 (Fig. S1) for NOAA stations at Tongue Point (No. 9439040) and Vancouver, Washington (Rkm-170; No. 9440083), are analyzed to give constituent and admittance estimates, using both CWT_Multi and NS_Tide (Matte et al. 2013). These results are compared to discharge data to show how the two tidal analysis approaches represent constituent variations during freshet events.

b. The SFBD

The Sacramento–San Joaquin Delta is composed of numerous interconnected river channels and drains more than a quarter of the state of California into San Francisco Bay (Figs. 4b,d). Tides are mixed, with mean and great diurnal ranges of 1.25 and 1.78 m, respectively, in San Francisco. Tides from the Pacific Ocean propagate far into the delta, with greater attenuation typically occurring along the larger, northerly Sacramento River (mean discharge, 550 $m^3\ s^{-1}$) than along the southerly San Joaquin River (mean discharge, 100 $m^3\ s^{-1}$). Substantial quantities of water are pumped from the southwest portion of the Delta to the California Water Project (average rate of ~200 $m^3\ s^{-1}$; see, e.g., Knowles 2002). During low discharge conditions, salinity can intrude into the delta (e.g., Monismith et al. 2002), compromising water quality. To reduce salinity intrusion, a temporary barrier was constructed in May 2015 and removed in October/November 2015 on a western delta channel, False River (~102 km from the Golden Gate; see Kimmerer et al. 2019, Fig. 4b). It was installed again in 2021 and 2022. The 2015 barrier provides an ideal test case to assess nonstationary analysis techniques and may provide insight into how other such structures affect tides, e.g., the more than 300 "salt barrages" constructed in China (Tilai et al. 2019).

Water-level data for the SFBD are taken from San Francisco (NOAA No. 9414290) and False River near Oakley (U.S. Geological Survey gauge No. 11313440) for January 2014–December 2017 (Fig. S2). This 4-yr time window includes a salt barrier closure during a severe drought and a series of storms and subsequent flooding in northern California in January–February 2017 (Downing-Kunz et al. 2021). The salt barrier led to relatively sharp changes in flow, while the flooding had a more gradual onset and abatement. These data are analyzed to compare CWT_Multi analysis results to those from a short-term HA (STHA; cf. Jay and Flinchem 1999). Our STHA uses a core of the UTide harmonic analysis package (Codiga 2011) to perform a 30-day HA every 20 h. This window allows for the resolution of all major constituents that are considered by CWT_Multi.

c. Artificial data generation

Two artificial time series were created to test CWT_Multi in a situation with known amplitudes and phases. The first is composed of stationary data with $|M_2| = 1$ m and other major constituent amplitudes normalized to M_2 per their amplitudes in the tidal potential (per Foreman 1977); phase lags are arbitrary but constant. Overtide amplitudes are similar to those in the LCRE and SF Bay. In the second record, M_2 is modulated as it might be by river flow, with artificial freshets of 7, 14, and 31 days. Default CWT_Multi filter frequencies and lengths are given in Table S1. Both datasets have energy at the 32 tidal frequencies (Table S2), plus random noise with an root mean square (RMS) of $0.05 \times |M_2|$.

d. Recent nonstationary tidal analysis code

The strong response of LCRE tides to nontidal forcing has allowed it to serve as a testbed for tidal analysis programs. Programs/analysis approaches tested include wavelets (Jay and Flinchem 1997; Flinchem and Jay 2000), robust T_Tide (Leffler and Jay 2009), NS_Tide (Matte et al. 2013), empirical mode decomposition (EMD) (Pan et al. 2018a; Pan and Lv 2019), S_Tide (Pan et al. 2018b), and variational mode decomposition (VMD) (Gan et al. 2021). VMD, like previous CWT analyses, determines tidal species behavior, whereas T_Tide, NS_Tide, and S_Tide analyze for tidal constituents.

The above methods are regression-based, EMD, VMD, and wavelets aside; thus, they lack a well-defined frequency response, and the output at any frequency depends on what other frequencies (constituents) are included in the analysis (Jay and Flinchem 1999), as well as on the data. Robust T-Tide differs from conventional T_Tide (Pawlowicz et al. 2002) only in the use of the iteratively reweighted least squares (IRLS or robust inversion) method to limit the influence of the outliers on the regression parameter estimates. The two HA methods used here, UTide (Codiga 2011) and NS_Tide (Matte et al. 2013), use robust inversion, and UTide embeds nodal corrections in its formulation following Foreman et al. (2009), while NS_Tide stands out for its use of physical forcing factors like river flow and coastal tidal range to construct basis functions that represent time-varying tidal parameters.

4. Results

a. Artificial data results

We first analyze artificial data with known frequency content as a means to assess the performance of CWT_Multi (Fig. 5). The estimated amplitudes and phases for the D_2 constituent groups N_2, M_2, and S_2 match the expected values, but are not constant, because N_2 and S_2 properties reflect the influence of the smaller group constituents ν_2 and K_2, respectively. The diurnal K_1 is similarly perturbed by P_1 and Q_1 by Rho_1. Removal of the influence of small constituents by dynamic inference is discussed below.

M_2 amplitude responds to fluctuations in river flow, while other constituents are less affected (e.g., Jay and Flinchem 1997; Godin 1999; Buschman et al. 2009; Moftakhari et al. 2013, 2016).

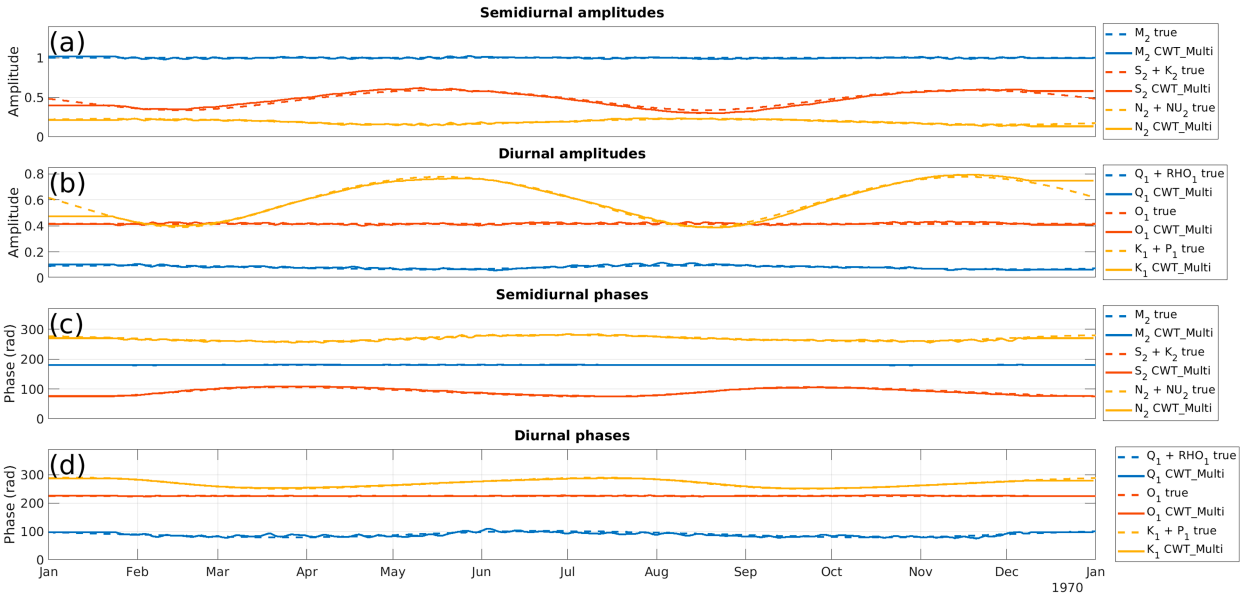

FIG. 5. Fortnightly constituent group analysis results for 1 year of stationary artificial data (date arbitrary) constructed from 32 constituents: (a) D_2 amplitudes, (b) D_1 amplitudes, (c) D_2 phases, and (d) D_1 phases. For groups that are strongly modulated by the presence of multiple strong constituents, the sum of the two largest inputs is plotted for reference. The RMS background noise was 5% of M_2 amplitude. Startup effects invalidate results for half a LOF at the beginning and end of the time series.

We consider, therefore, 1 year of artificial data that includes abrupt freshet events of the duration of 7, 14, and 31 days, respectively, during which M_2 amplitude drops abruptly by 40% (Fig. 6a). The CWT_Multi species outputs follow the input very closely (Fig. 6b). The constituent solution captures the occurrence and character of the events, but smooths out the step function decrease in M_2 amplitude (Figs. 5a,c). The longer the event, however, the better the results. Species filters better follow the time evolution of the events, but cannot show that M_2 acts differently from other constituents. Further CWT_Multi properties are demonstrated using real data, with comparisons to other analysis approaches.

b. *LCRE results*

1) ASTORIA

Species analysis (Fig. 7) results show the expected tidal monthly variations and a modest response to river flow; they

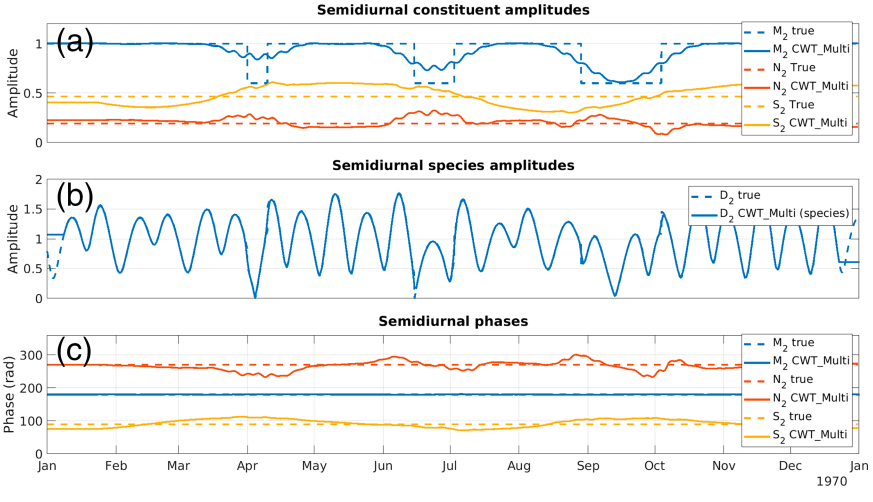

FIG. 6. Fortnightly D_2 analysis results (three major constituents) for 1 year of artificial data (date arbitrary) constructed from 32 constituents; amplitudes and phases are constant, except that M_2 amplitude varies as shown (dashed line in Fig. 6a); input and calculated: (a) D_2 constituent amplitudes, (b) D_2 species amplitudes, and (c) D_2 constituent phases. The noise level is as in Fig. 5.

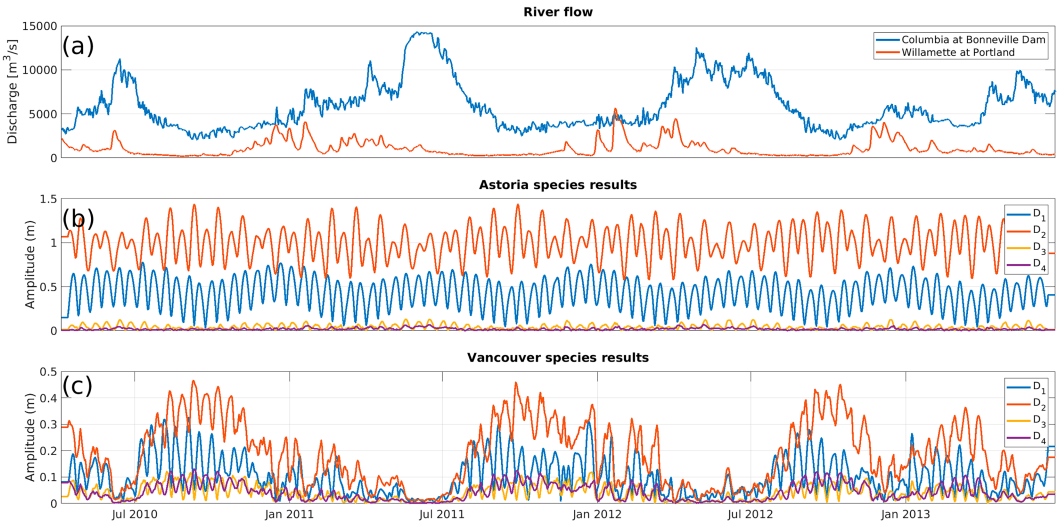

FIG. 7. LCRE river inflow and tidal properties from April 2010 to June 2013: (a) river inflow from the main stem Columbia and the Willamette in Portland Harbor; (b),(c) CWT_Multi analysis for species D_1–D_4, for Astoria and Vancouver.

provide the best reconstruction (Table 1) but obscure the behavior of individual constituents. Fortnightly constituent group analysis results (Figs. 8 and 9) are typically more useful here and in other situations where nonstationarity is modest. The fortnightly CWT_Multi D_1 constituent group analyses show expected twice-yearly modulations caused by multiple group constituents that are not individually resolved. For example, the CWT_Multi K_1 group output varies by ~0.06 m, reflecting the interaction of (primarily) K_1 and P_1. Similarly, O_1 group amplitude varies around its mean by about ±0.025 m at the beat frequency of 2 cycles per year due to the influence of τ_1 and amplitude of ~0.025 m. CWT_Multi also shows that the O_1 group decreases from 2010 to 2013, due to the 18.6-yr nodal cycle variation of O_1 (about 19%; Cartwright and Edden 1973). This trend is not shown by NS_Tide, because nodal modulation corrections were not implemented; instead, modulation by river flow is the main source of variability. The two groups separated by only 1 cycle per month (Q_1 and O_1) show 7–14-day oscillations that apparently represent beating between several constituents. These can be removed, either by using the redundancy of the outputs to time average over the time scale of the filter (~1 week, useful for plotting) or by increasing filter length for the smaller constituent, in this case, Q_1. Figure S3 suggests that Q_1 results here can be improved by setting the Q1 filter length to 45 days.

D_2 constituent group fortnightly outputs from CWT_Multi show phenomena similar to those for D_1 groups (Fig. 9); e.g., the N_2 and S_2 groups show the expected approximately semiannual perturbations by N_2–ν_2 and S_2–K_2 superposition, respectively (cf. Pan et al. 2023a). There are also fortnightly variations in the S_2 group output that may be nonphysical or related to changes in frictional interactions over the neap–spring cycle, which causes considerable variation in salinity intrusion and bed friction (Kay and Jay 2003). Weekly fluctuations in the M_2 and N_2 groups are caused by the strong overlap of their filters. The primary variations (decreases) in M_2 are driven by annual spring flow events with smaller decreases in winter (Fig. 9a). Overall, there is good agreement in mean values between the CWT_Multi and NS_Tide analyses in both the D_1 and D_2 bands. Phase results analogous to Figs. 7 and 8 are provided in Figs. S4 and S5. Among the overtides, M_4 amplitudes show close agreement between CWT_Multi and NS_Tide, while for MK_3, mean amplitudes are similar within 10%,

TABLE 1. RMSE for reconstruction of input data, by location and analysis method.

Lower Columbia River				
Station	NS_Tide RMSE (m)	CWT_Multi species RMSE (m)	CWT_Multi constituent RMSE (m)	UTide RMSE (m)
Astoria	0.0919	0.0231	0.0475	0.0545
Vancouver	0.0790	0.0295	0.0753	0.0807
San Francisco Bay				
Station	UTide RMSE (m)	CWT_Multi species RMSE (m)	CWT_Multi constituent RMSE (m)	
False River	0.0379	0.0148	0.003 34	
San Francisco	0.0304	0.0169	0.002 79	

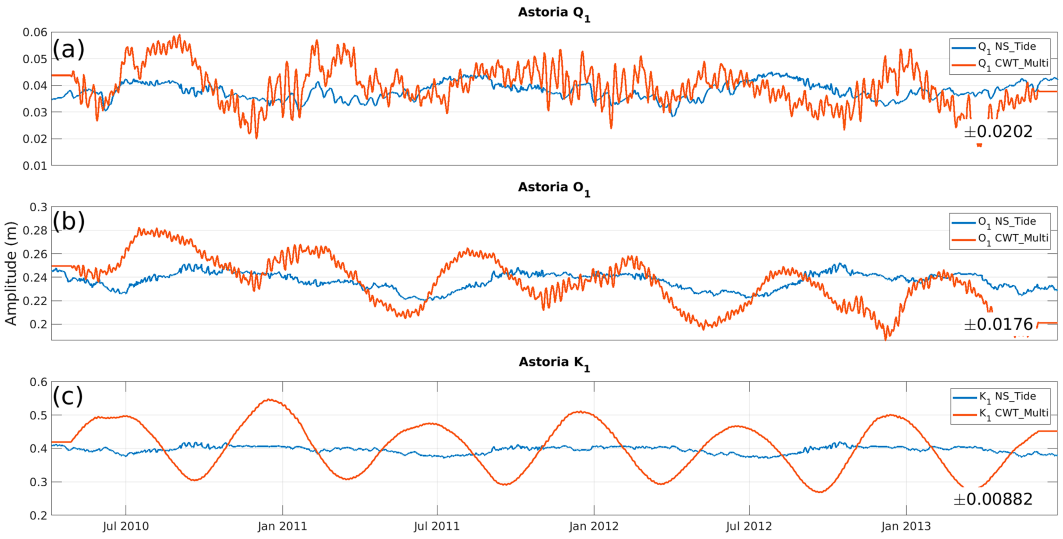

FIG. 8. CWT_Multi fortnightly amplitudes at Astoria for the (a) Q_1, (b) O_1, and (c) K_1 constituent groups, with comparison to NS_Tide; CWT_Multi 95% confidence limits estimated by the residual spectrum method (RSM) are shown at the lower right of each panel, here, and in subsequent figures.

but time histories differ, probably because of a difference in the constituents analyzed (Fig. S5).

2) VANCOUVER

Vancouver data are a useful test of analysis methods because subtidal water levels rise and fall by 3–6 m seasonally (Fig. S1b; Jay et al. 2011, 2014), and constituent group amplitudes vary by an order of magnitude (Figs. 10 and 11). Twice-yearly variations occur for both the D_1 and D_2 species, but are obscured by fluctuations due to river flow. Comparison of the constituent group results in Figs. 10 and 11 to the species results in Fig. 7c suggests that the constituent results illuminate the diverse behaviors of individual constituents, but do not follow rapid flow fluctuations as well as the species results or NS_Tide, e.g., during the rapid rise in flow in spring 2011 or the winter floods early in 2012. CWT_Multi and NS_Tide agree fairly well overall, including for major D_3 and D_4 overtides (Fig. 12), though the MK_3 group shows some differences, and there are tidal monthly oscillations in the NS_Tide outputs. It is typical of tidal rivers that overtides grow as the tide propagates landward (e.g., Jay et al. 2014; Hoitink and Jay 2016; Guo et al. 2015); thus, overtides are larger at Vancouver than Astoria. Analogous phase analysis results are provided in Figs. S6 and S7. Interestingly, the M_2 and O_1 waves are delayed by increased flow (as expected), but the K_1 wave is accelerated, suggesting O_1–K_1–M_2 triad interactions; this

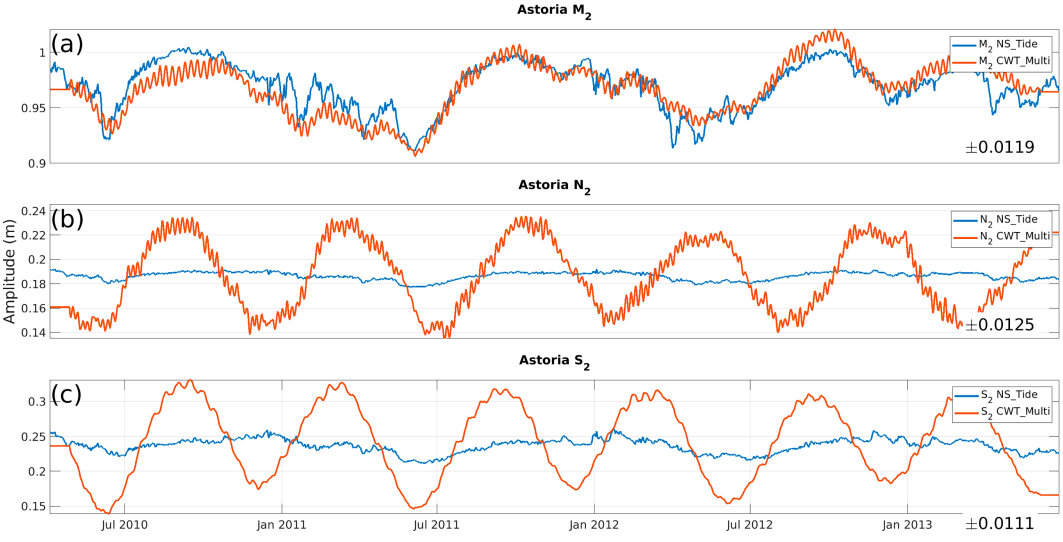

FIG. 9. CWT_Multi fortnightly amplitudes at Astoria for the (a) M_2, (b) N_2, and (c) S_2 constituent groups, with comparison to NS_Tide; mean CWT_Multi RSM 95% confidence limits are shown as in Fig. 7.

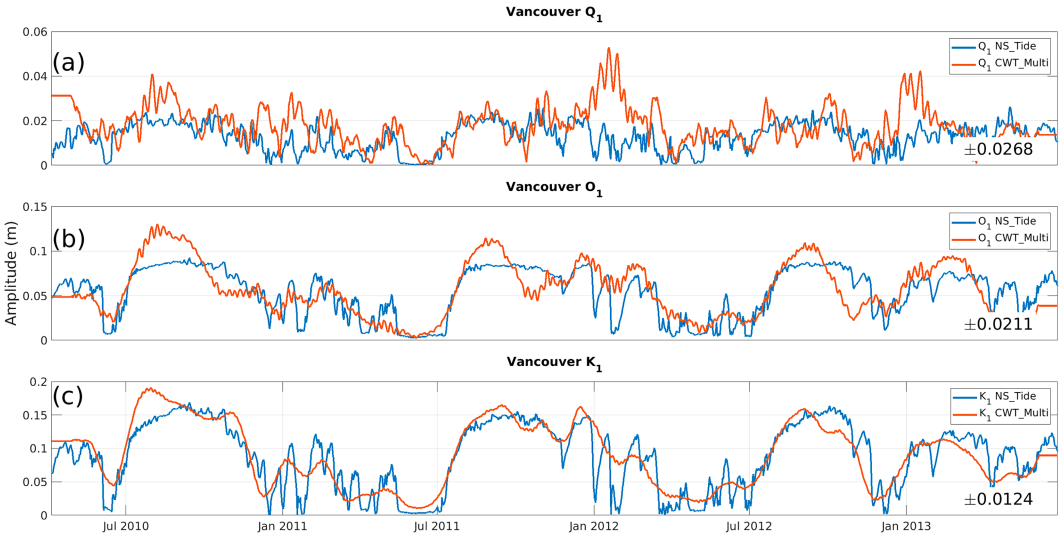

FIG. 10. CWT_Multi fortnightly amplitude results at Vancouver for the (a) Q_1, (b) O_1, and (c) K_1 constituent groups, with comparison to NS_Tide results; CWT_Multi RSM 95% confidence limits as in Fig. 8. The confidence limits suggest that the Q_1 and sometimes even the O_1 results cannot be distinguished from zero; this is typical for river tides during high-flow periods.

illustrates the utility of extending CWT tidal analysis to the constituent level.

3) RECONSTRUCTION AND DETIDING

Reconstruction of analyzed and residual (observed–reconstructed) time series is vital for both error estimation and providing a "detided" time series, i.e., a nontidal residual (NTR). CWT_Multi reconstruction is quite successful for Astoria; constituent and species reconstructions outperform NS_Tide in the tidal band by ~1.9× and 4×, respectively (judged by RMSE; Table 1 and Fig. 13). At Vancouver, NS_Tide and the CWT_Multi constituent group analyses have similar reconstruction RMSE values, while the CWT_Multi species analysis reduces the RMSE by 2.7×. This result highlights the advantage of using wide species filters in a highly nonstationary application. However, NS_Tide reconstructs tidal monthly phenomena in addition to the main tidal bands, while CWT_Multi focuses at present only on the main tidal bands. A reconstruction based on UTide STHA provided reconstruction results almost as good as the CWT_Multi

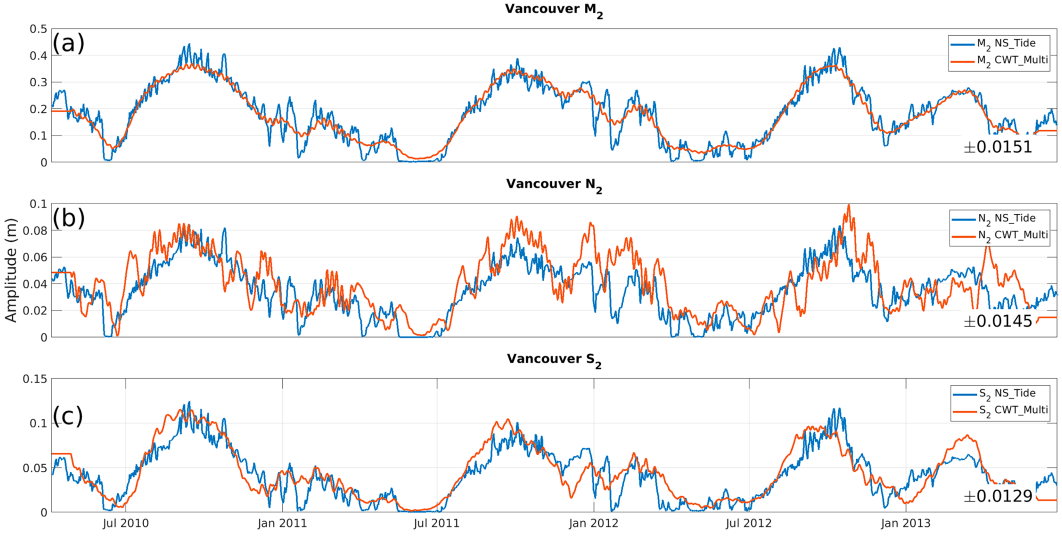

FIG. 11. CWT_Multi fortnightly amplitude results at Vancouver for the (a) M_2, (b) N_2, (c) and S_2 constituent groups, with comparison to NS_Tide results; CWT_Multi RSM 95% confidence limits are shown; the N_2 and S_2 confidence limits sometimes include zero during high-flow periods. During the highest flows in the spring of 2011, even M_2 is marginally significant, and the tide almost disappears.

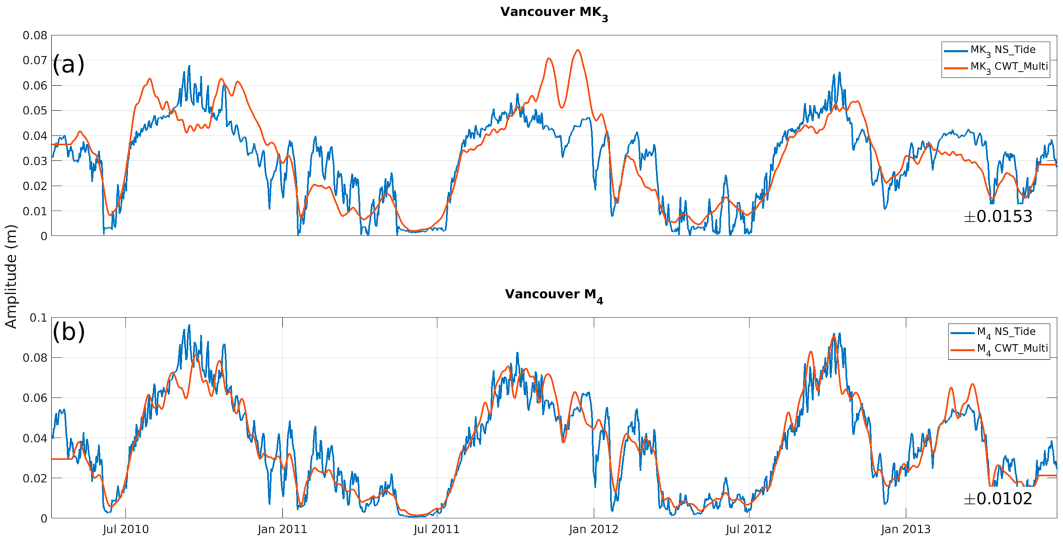

FIG. 12. CWT_Multi fortnightly amplitude results at Vancouver for (a) MK_3 and (b) M_4; the CWT_Multi RSM 95% confidence limits (as in Fig. 8) for both constituents sometimes include zero.

constituent solution at Astoria (Table 1), but the UTide RMSE was still larger by ~2.3–2.7× (depending on the station) than that from the CWT_Multi species solution. From a spectral perspective, CWT_Multi and NS_Tide are both effective at detiding (at least for the D_1–D_4 band analyses by NS_Tide) (Fig. 14).

c. *San Francisco Bay and Delta results*

The closure of the False River channel between May and November 2015 and a large discharge event between January and March 2017 provide opportunities to examine nonstationary tidal behavior in the SFBD system (Fig. 15). Most results are from the False River station near the salt barrier, but comparison of False River and San Francisco results, the latter less affected by river flow, offers insight into the use of the admittances provided by CWT_Multi.

1) FALSE RIVER

The effects of the two SFBD events (the salt barrier in spring–summer 2015 and the flood of winter 2017) are gradual enough that they can be resolved by the CWT_Multi constituent group analysis (Figs. 15 and 16); species analysis results are shown in Fig. S8. CWT_Multi and UTide results for D_1 and D_2 constituent groups are similar; O_1 and K_1 results suggest that barrier closure decreases D_1 and D_2 amplitudes by tens of millimeters. Interestingly, all the D_2 groups except M_2 show large fluctuations for several weeks, while the salt barrier was installed and removed (May and November 2015).

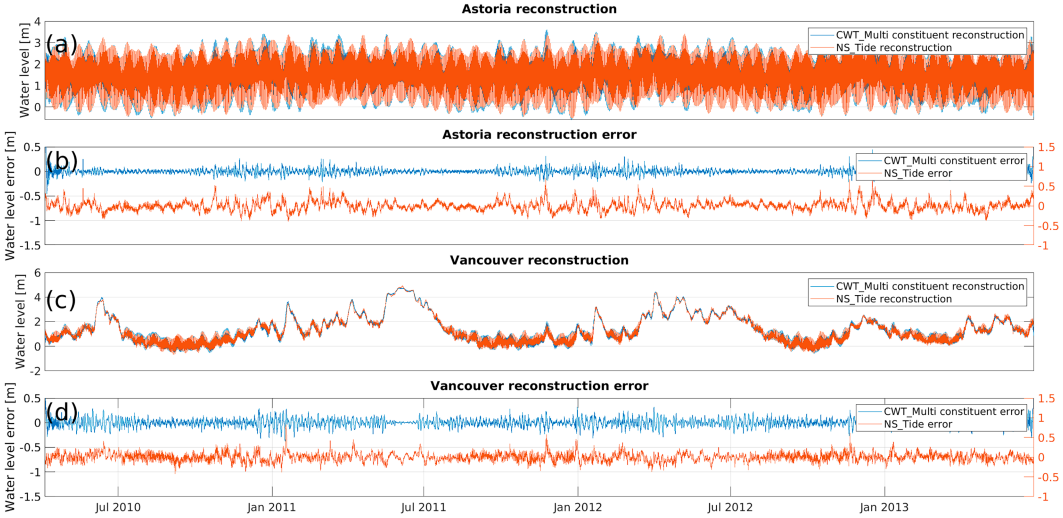

FIG. 13. (a),(b) Reconstruction results and RMSE for Astoria as provided by CWT_Multi and NS_Tide; and (c),(d) as in (a) and (b), but for Vancouver.

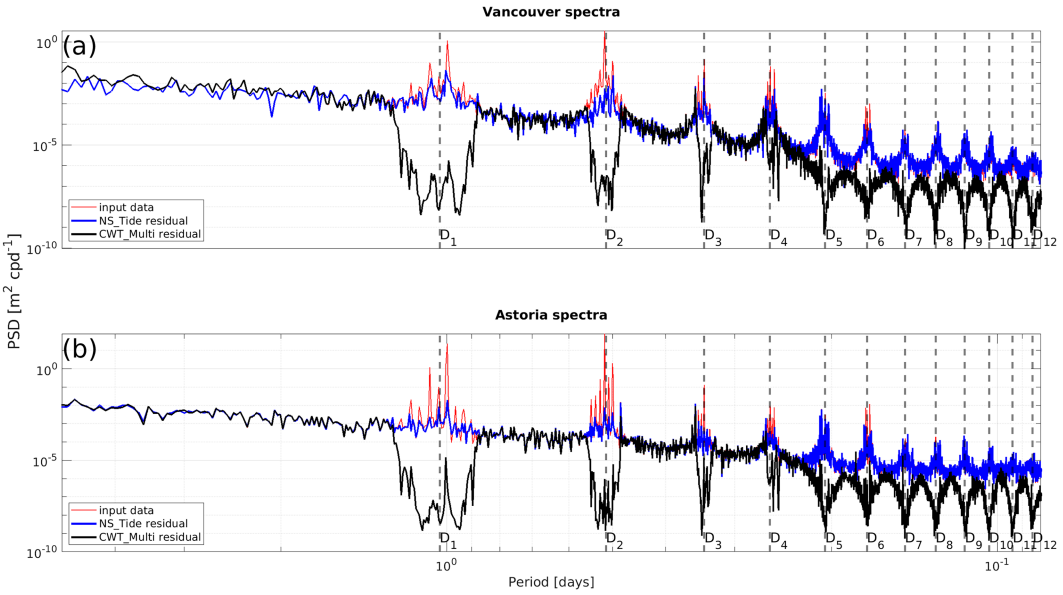

FIG. 14. Water-level power spectra for (a) Vancouver and (b) Astoria, for the input data and the residual after removal of tides, the latter for NS_Tide and the CWT_Multi constituent analysis.

Phase results show a delay (larger phases) for both D_1 and D_2 constituent groups following barrier closure, suggesting reflection or that the tidal wave traveled a different, longer path (see Fig. 4b, Figs. S9 and S10). The winter 2017 flood reduces M_2 amplitude at the peak of the flow (as expected, Fig. 16a). CWT_Multi and UTide results for overtide constituent groups MK_3 and M_4 are provided in Fig. S11. Again, the two approaches generally agree; M_4 is depressed during the barrier closure, perturbed before the winter freshet, and augmented during the high flows of January–February 2017. MK_3 is slightly larger during the freshet.

Finally, CWT_Multi resolves the L_2 group quite well; its amplitude (0.023 m) is 4.7 times the 95% confidence limit, and SNR = 9.2 (Tables S5 and S7). Whether L_2 and constituent groups of similar magnitude (e.g., μ_2, J_1, and NO_1) can be resolved by CWT_Multi in other situations depends on background noise and constituent ratios in the system analyzed.

Reconstruction and detiding results for the SF Bay stations are similar to those for the LCRE stations. The CWT_Multi constituent and UTide reconstructions have RMSE values that are ~1.6–2.5× higher than the CWT_Multi species

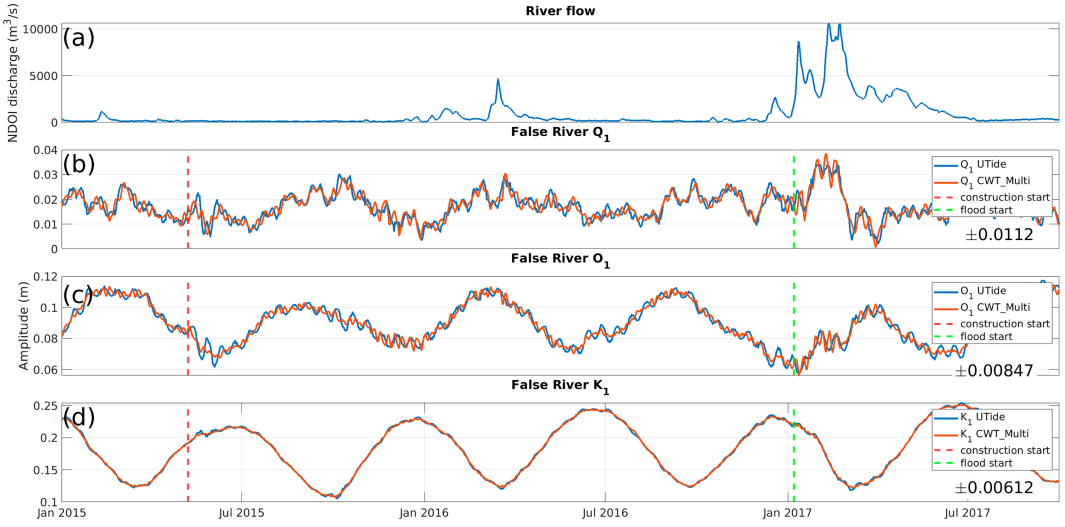

FIG. 15. (a) Net delta outflow index (NDOI) river inflow to SF Bay; CWT_Multi fortnightly amplitude results at False River for the (b) Q_1, (c) O_1, and (d) K_1 constituent groups, with comparison to UTide; CWT_Multi RSM 95% confidence limits are shown as in Fig. 8; Q_1 is sometimes not distinguishable from zero, but O_1 and K_1 almost always are.

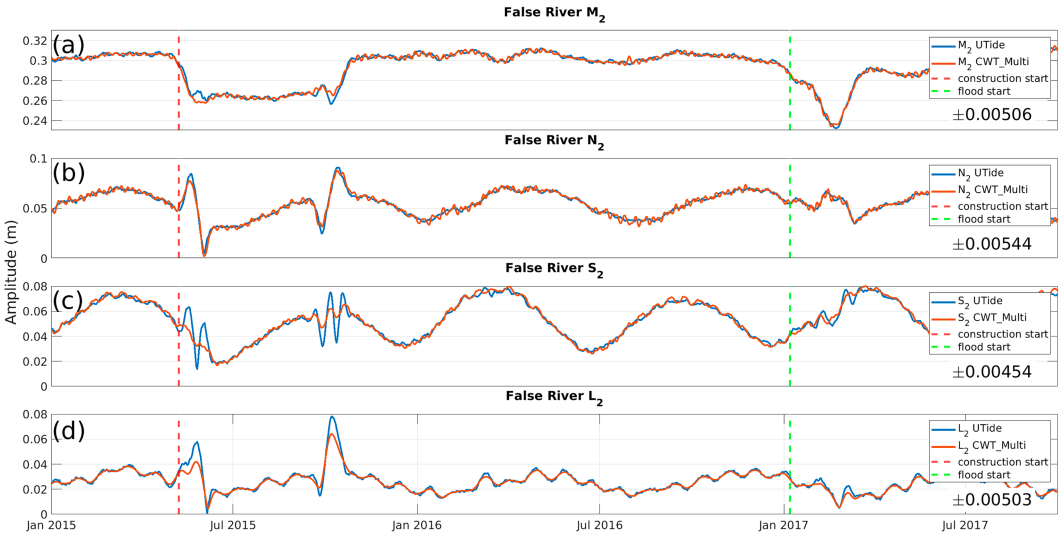

FIG. 16. CWT_Multi fortnightly amplitude results at False River for the (a) M_2, (b) N_2, (c) S_2, and (d) L_2 groups; CWT_Multi RSM 95% confidence limits are shown; the N_2 and L_2 amplitudes are sometimes not distinguishable from zero.

reconstruction (Table 1). The residual spectra in Fig. 17 suggest that CWT_Multi and UTide perform similarly (and quite successfully) in the D_1 and D_2 bands, but that CWT_Multi better captures the highly variable behavior of overtides. Detailed results for SF are provided in Figs. S12–S16.

2) ADMITTANCE

Calculation of a tidal admittance sometimes clarifies dynamics, by removing the influence of constituents not resolved on those analyzed. Figure 18 illustrates this point. Using the San Francisco gauge record as a reference, M_2 admittance amplitude drops by ~15% during the salt barrier period (spring–summer 2015), but increases slightly (after an initial drop) during the January–February 2017 flood period, despite a decrease in M_2 group amplitude at False River. This increase implies that M_2 amplitude was more affected (or affected for a longer time) at San Francisco than at False River, which is located away from the main Sacramento River flow. If, on the other hand, M_2 admittance amplitude is estimated relative to η, a decrease is seen during the flood. Clearly, there are interesting dynamics to investigate here, and the admittance can be a useful tool.

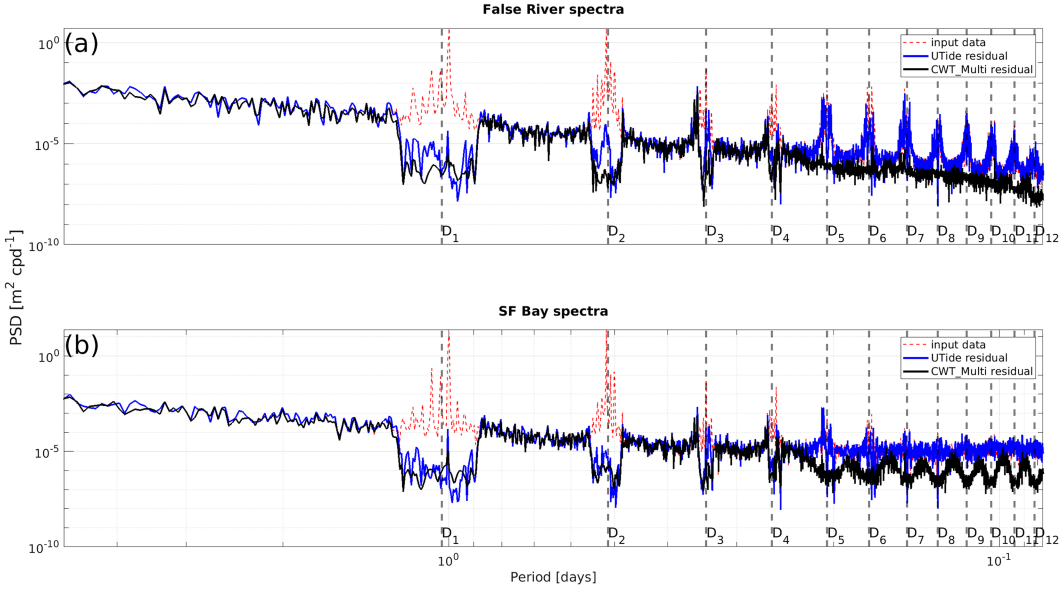

FIG. 17. Water-level power spectra for (a) False River and (b) San Francisco for the input data and for the residual after removal of tides, the latter for NS_Tide and the CWT_Multi constituent analysis.

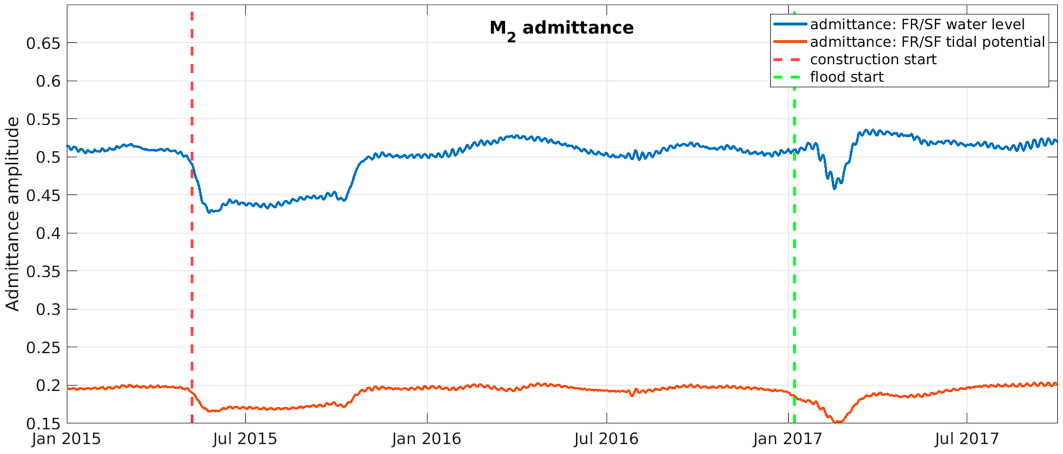

FIG. 18. M_2 admittance amplitude at False River estimated relative to the tidal potential η and to the San Francisco Station; see text for interpretation.

In summary, SF Bay analysis results show that tidal estimates from CWT_Multi and UTide are similar, but that CWT_Multi provides better reconstruction and better resolves overtides, while providing excellent time resolution of tidal behavior. The superior reconstruction ability of CWT_Multi under nonstationary conditions is advantageous for detiding and may be useful for short-term prediction, if future forcing can be estimated. Its admittance calculation is also useful for understanding dynamics.

d. *Dynamic inference*

We demonstrate the possibilities of CWT_Multi dynamic inference using the K_1 group in the highly nonstationary Vancouver record (Fig. 19). Of interest at this station is the diel flow variability introduced by variable power production at Bonneville Dam, 60 km further landward (Jay et al. 2016). The diel input (period 24 h) is irregular, but has the same frequency as tidal constituent S_1, which differs from K_1 and P_1 by ± 1 cycle per year. The power peaking signal propagates downriver at least 140 km as a longwave (Jay et al. 2016). Within the K_1 group, K_1, S_1, and P_1 can be separated with seasonal filters, allowing the use of dynamic inference at the fortnightly scale. We see that S_1 is almost always larger than P_1 and sometimes nearly as large as K_1 at Vancouver, and the fortnightly estimates show considerable time variability, presumably due to variations in power production. The fact that the fortnightly results resemble the seasonal results, but with more detail, suggests that the fortnightly calculation is stable. While these preliminary results are intriguing, a thorough study of power peaking would require analysis of the flow record to determine the time scales of flow variability, and careful optimization of CWT_Multi for this situation, tasks beyond our present scope. Further examples of dynamical inference are provided in Figs. S18 and S19.

e. *SNR and constituent selection*

CWT_Multi provides SNR values and postanalysis constituent selection via the Munk–Hasselmann criterion and its modification [Eqs. (5a) and (5c), respectively]. For Astoria and Vancouver, respectively, 26 and 25 of 32 constituents have

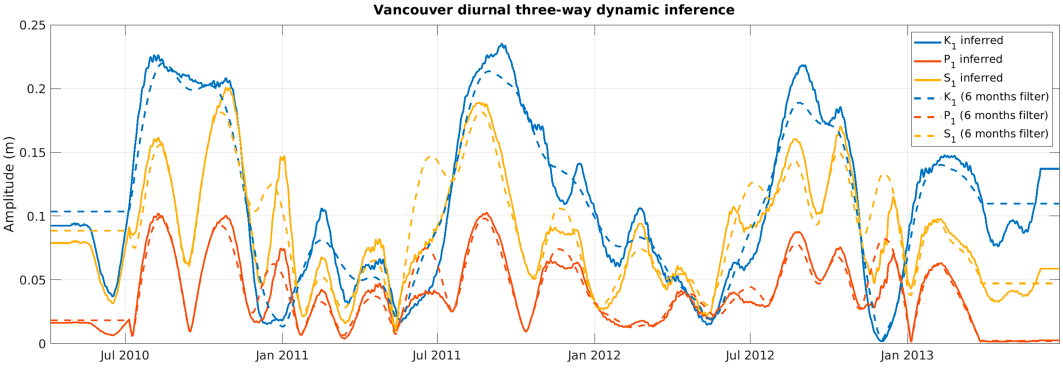

FIG. 19. Dynamic inference results for the K_1 constituent group (constituents K_1, S_1, and P_1) for Vancouver; end effects are evident in the first and last 3 months. The pronounced annual cycle stems from the damping effects of the annual river flow cycle. The unusually strong S_1 signal (generally larger than P_1) stems from diel power peaking at Bonneville Dam.

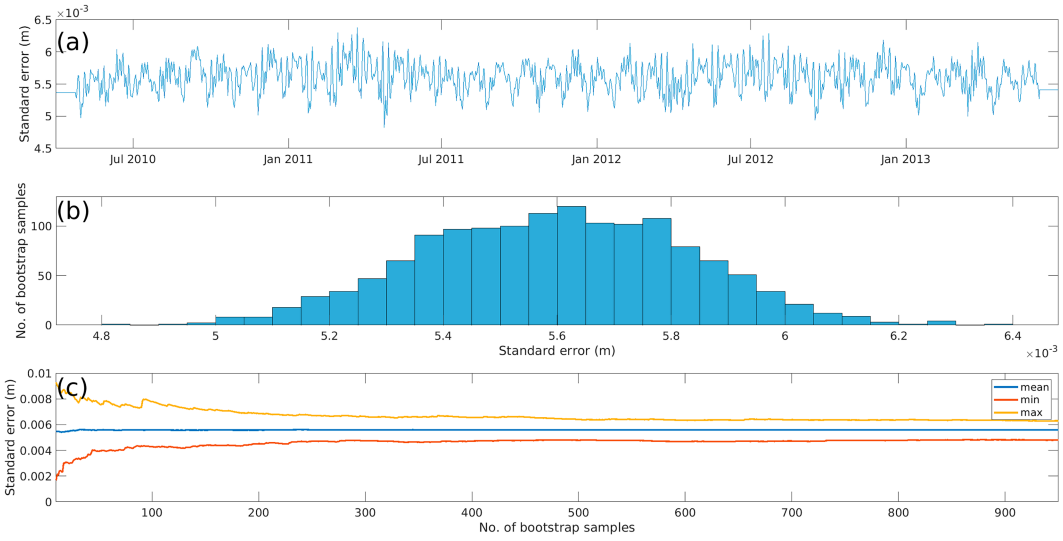

FIG. 20. MBB error analysis for M_2 at Astoria: (a) time series of standard error; (b) histogram of standard error; (c) convergence of minimum, mean, and maximum standard error estimates over the 1000 MBB resamples as a function of number of bootstrap samples.

SNR ≥ 2 (Table S3). Using $C_R = 1$ in Eq. (5c), 29 of 32 are well resolved (i.e., have $\Delta f_i \leq 0.03$ cycle per day ≈ 1 cycle per tidal month) at Astoria and 28 of 32 are well resolved at Vancouver. For False River and San Francisco, respectively, all but eight and six SNR ratios are SNR ≥ 2. In terms of Eq. (5c), almost all constituents are well resolved at both stations. CWT_Multi results are compared to NS_Tide and UTide in Tables S3–S7. The seasonal variability of the LCRE data, including the near disappearance of tides at Vancouver during high-flow periods, suggests that time-variable SNR and constituent selection would be a useful addition to the program. Both are possible using the standard error estimates at each time step (Fig. 20).

f. *Uncertainty analysis*

CWT_Multi provides two approaches to assess the uncertainty of parameter estimates: a moving block bootstrap (MBB) method and a residual spectrum analysis (SRM). To illustrate how MBB works, Fig. 20a shows a time series of standard errors for M_2 at Astoria, Figure 20b shows a histogram of these results, and Fig. 20c shows that MBB standard error estimates converge to about 0.0056 m as the number of iterations increases; the corresponding estimate from the SRM is 0.006 m. In contrast to Innocenti et al. (2022), the MBB standard error for M_2 varies only slightly after about the first 300 realizations. This pattern may result from a difference between HA (used by Innocenti et al.) and wavelet analysis. HA sets up a least squares problem over the whole length of the record, while CWT_Multi estimates are local. CWT_Multi constituent group estimates are made within a time window that is smaller than the residual blocks of the MBB method, but the frequency response is narrow enough (in the spectral sense) that the signal is much more energetic than the background noise. Thus, the CWT filters see approximately the same data, regardless of the orders of the blocks. Another way to explain this result is that it stems from the linearity of wavelet filters—the estimate for any given filter is nearly independent of the content of the signal in other spectral bands.

Interestingly, MBB suggests a smaller uncertainty estimate than the SRM approach for the constituent analysis, but a larger confidence interval for species analysis (Table 2). This occurs because the species filters are relatively wide and capture considerable tidal energy near their central frequency. This leads to low energy in the residual data around their respective frequencies and low SRM estimates of error based on residual variance.

MBB captures this situation differently, by constructing dataset realizations that contain different background energy levels in different local windows. Thus, the wide frequency response of wide CWT filters causes them to be susceptible to uncertainty based on the variable noise around tidal bands. From these results, the desire for a conservative evaluation of uncertainty in tidal properties suggests the use of MBB for species analysis confidence intervals, whenever computational constraints allow. Interestingly, the width of the filters that increases MBB uncertainty estimates facilitates reconstruction under nonstationary conditions. Thus, while tidal species estimates may be uncertain in the bootstrap sense, that does impair their utility. Further confidence limit results are provided in Tables S7 and S8.

g. *Computation time*

CWT_Multi computation time for one time series (Astoria, length 3.25 year) with reconstruction, inference, and SRM error estimates was 44 s and without inference was 32 s. If, however, the MBB is implemented, computing time is about 5 h. UTide computation time for the 4-yr record False River record was 44 s. These times are for a laptop with four cores running at 1.6 GHz and 8 GB of RAM. NS_Tide required 494 and

TABLE 2. Comparison of confidence limits for Astoria for the SRM and the MBB, based on 750 permutations. The M_2 and D_2 results are from the constituent and species analyses, respectively.

Method	M_2 SRM	M_2 MBB	D_2 SRM	D_2 MBB
CI (m)	0.005 95	0.003 23	0.005 34	0.0768

305 s for Astoria (53 constituents) and Vancouver (39 constituents), respectively, for 3.25-yr records, using four cores at 2.7 GHz with 32 GB of RAM.

5. Discussion

a. A well-formed tidal analysis method

New tidal analysis methods are being developed at a rapid rate (cf. Jay et al. 2022). Most of these have potential but are of limited utility at present, due to lack of flexibility, error estimates and other tidal analysis components, and/or excessive computing time. We suggest that a well-formed tidal analysis method should provide, in addition to amplitude and phase estimates at a set of tidal frequencies, 1) a constituent selection criterion suitable for nonstationary data; 2) flexibility with respect to the constituents or frequencies analyzed; 3) accommodation of gappy data; 4) analysis of nonstationarity on a variety of time scales; 5) calculation of astronomical phases; and 6) estimation of SNR and confidence limits. Other desirable properties include calculation of tidal admittances, inference, multiple viewpoints of the data analyzed, time-dependent uncertainty estimates, and an ability to analyze irregularly spaced and extremal data. Functionality for infrequently sampled data (e.g., from altimetry) is also useful. Our aim here is to emulate Pawlowicz et al. (2002), Foreman et al. (2009), Codiga (2011), and Matte et al. (2013) by providing a practical code, CWT_Multi, suitable for users that are not tidal specialists. Accordingly, we provide most of the above elements, but CWT_Multi cannot analyze extremal (high–low) data because it requires a uniform sampling interval, and it does not presently provide time-variable uncertainty estimates.

b. The role of CWT_Multi

These "desirable" tidal analysis properties emerge from consideration of five dilemmas that arise in the analysis of nonstationary tidal records. Understanding how CWT_Multi navigates these problems provides a useful overview of this work and, we hope, a roadmap for future efforts. The first dilemma is the trade-off between time and frequency resolution expressed by the Heisenberg uncertainty principle (Rioul and Vetterli 1991; Flinchem and Jay 2000):

$$\Delta f \times \Delta t \geq (4\pi)^{-1}, \tag{6}$$

where Δf and Δt are the normalized frequency and time uncertainties, respectively. All tidal analysis methods evade Eq. (6) to some degree by asserting that the frequencies are a priori known, but the time-dependent behavior of closely spaced frequencies remains difficult to resolve, because time dependence is equivalent to the spreading of spectral peaks. CWT_Multi's separation of multiple tidal constituents within tidal species changes the use of Eq. (6), relative to earlier CWT approaches. Instead of scaling filter lengths inversely with frequency to optimally resolve time variations and limit redundancy, filter lengths are independent of absolute frequency because of the need to resolve closely spaced (at 1–2 cycles per month) constituents within each tidal species. All frequencies have the same decimation, and outputs are highly redundant, which facilitates data analysis and smoothing of outputs for plotting.

Second, the nontidal components of a signal limit the frequency resolution of tidal signals. The conventional rule (the Rayleigh criterion R_C) for constituent selection in HA requires that $\Delta f \approx \mathrm{LOR}^{-1}$, a restatement of Eq. (6). Thus, two frequencies differing by 1 cycle per year require a 1-yr record for their resolution, for $R_C = 1$. MH64 shows that the presence of noise fundamentally changes the way that frequency selection should be considered. Taking $\Delta t \approx$ (LOR/const), the MH64 criterion [Eq. (5a)] is a generalization of Eq. (6). Applying Eq. (5a) is difficult in HA, because the SNR is not known prior to analysis. Here, CWT linearity guarantees that CWT_Multi outputs at any given frequency are independent of those at other frequencies. Thus, constituent selection via Eqs. (5a) and (5c) can be performed as a postprocessing step, rather than through iterative analyses, as is desirable with HA. Finally, CWT_Multi focuses on resolving tidal species on time scales of a few days and constituent groups on a fortnightly basis. This is an extension of the idea in Jay and Flinchem (1997) that tidal species are more fundamental than constituents—CWT_Multi views the frequency structure of a time series on multiple time scales. If the system is very nonstationary, constituent estimates are not meaningful, and CWT_Multi allows the user to evaluate this issue.

Third, there is the question of how much physics to put into an analysis method. Most tidal analysis approaches assume that tidal frequencies are known, most HA methods relate constituent phases to the moon's passage over the Greenwich meridian, and some use the astronomical tidal potential (e.g., Munk and Cartwright 1966) as a basis for analysis. With nonstationary tides, information about nontidal forcing is pertinent, but should it be included directly in the analysis or employed, ex post facto, during the analysis of the output? CWT_Multi leaves the nontidal forcing for postprocessing analyses, but calculates complex admittances using the astronomical tidal potential and/or data from a coastal reference station, facilitating further analysis.

Fourth, tidal analysis methods confront the issue of prediction, historically the central purpose of tidal analysis (Cartwright 1999; Reidy 2008). Typical HA codes assume stationarity and use sine and cosine basis functions of infinite extent in time to allow predictions and hindcasts outside of the analysis period. An additional assumption that the behavior of constituents on time scales of 4.4–18.6 years can be estimated from the tidal potential is also questionable (Ray 2006), but is usually a minor problem in comparison with the assumption of stationarity. Thus, whether prediction is sensible is a physics question, external to any analysis code. The finite (in time) wavelets used by CWT_Multi do not include information about external forcing, though the tidal properties it outputs can be

regressed against external forcing (Jay et al. 2011, 2016). Thus, NS_Tide is a more practical prediction tool, because it builds nontidal forcing like river flow into its basis functions. Overall, the primary niches for CWT_Multi are to 1) facilitate dynamical analyses, 2) improve the time resolution of constituent group variability, and 3) reconstruct and detide data. CWT_Multi excels at these tasks because it offers outputs on multiple time scales, can respond to rapid changes in tidal properties, and does not inject a model of physical forcing into the basis functions.

Further, it is vital to have solid uncertainty estimates. Here, we provide both MBB (Innocenti et al. 2022) for amplitudes and a simpler and faster spectral residual analysis (SRM; Pawlowicz et al. 2002; Codiga 2011) for both amplitudes and phases. However, the optimum approach for phase confidence limits is not altogether obvious, because phase is a circular variable, to which the assumption of a normal distribution of residuals, central to the SRM, does not apply (Fischer 1993). Also, the SNR and confidence limits calculated by CWT_Multi are global (apply to entire time series), whereas these quantities vary over time (Fig. 19), as nontidal processes, data quality, and the astronomical tidal forcing vary. Thus, more work is needed on error analyses for nonstationary tides.

The above dilemmas constrain the choice of solution approach. With CWT_Multi, we maintain the superior time resolution of nonstationary tidal species provided by previous CWT codes, while also estimating the time-dependent behavior of a limited number of major tidal constituents in tidal species D_1–D_4. However, it is advisable to analyze nonstationary signals by multiple methods (Jay et al. 2014). Thus, we also provide power spectra, as well as CWT outputs on multiple time scales to maximize time resolution of nonstationary behavior. Comparison of CWT_Multi results to outputs from harmonic programs will also be useful in many circumstances.

6. Conclusions

Jay and Kukulka (2003) argued that nonstationary tidal behavior, though requiring new analysis techniques, provides an opportunity to analyze tidal dynamics in a new way. CWT_Multi expands on our ability to analyze these dynamics by providing improved access to the statistics of short-term tidal variability of constituents and, for highly nonstationary data, improved stability, signal-to-noise ratios, and reconstruction. CWT_Multi is flexible, and its filter lengths can be adjusted by the adventurous user.

Analyses of stations in San Francisco Bay and the Lower Columbia River suggest that for situations with moderate nonstationarity, constituent solution results will be similar to those from normal HA programs run in STHA mode. In situations with stronger nonstationarity, CWT_Multi still captures the time dependence of individual constituents, e.g., the behavior of K_1, S_1, and P_1 at Vancouver. Thus, CWT_Multi is a powerful, multipurpose tool that excels in dynamical analyses because it captures tidal species and constituent behavior on short time scales not accessible with most analysis codes.

Success in reconstruction/detiding is one important measure of a tidal analysis routine. Reconstruction based on the CWT_Multi species solution outperforms other approaches when the original data are strongly nonstationary, because it follows rapid nonstationarity and includes more of the tidal spectrum. For mildly nonstationary data, the constituent solution performs better than the species solution, probably because it follows the divergent behavior of individual constituents. Finally, CWT_Multi implements a modified MH64 frequency selection approach and provides a new form of inference (dynamic inference) that is based on evolving time series properties, not user input. Overall, CWT_Multi is a useful tool that can be employed to improve our study of nonstationary tides and related oceanographic phenomena.

Acknowledgments. David Jay acknowledges support from the Bonneville Power Administration through project 2002-077-00 led by the Pacific Northwest National Laboratory (PNNL). David Jay, Steven Dykstra, and Stefan Talke were supported by the California Delta Stewardship Council, Contract DSC-21024. Thanks to Tamara Dendall for programming the constituent selection component.

Data availability statement. The Innocenti et al. (2022) bootstrap package, parts of which are included in the CWT_Multi code, can be obtained from https://zenodo.org/record/7085587. The implementation of UTide used for nonstationary data analysis is available from https://github.com/mjclobo/moving_UTide. The CWT_Multi code has been placed on GitHub to facilitate further code development; see https://github.com/mjclobo/CWT_Multi. It is also available from the PSU Library repository at https://pdxscholar.library.pdx.edu/cengin_data/4/. All data used in this project are in the public domain, except those for Vancouver. After the submission of this paper, NOAA revised the 2002–21 Vancouver dataset. Changes in the data (old − new) ranged from about −0.01 to 0.09 m, with the largest changes during high-flow periods when tides were very small. Changes in CWT_Multi analyzed tidal constituents were in the 10^{-3}–10^{-4} m range. To facilitate the reproduction of our results, the 2010–12 Vancouver data used here have also been posted to https://pdxscholar.library.pdx.edu/cengin_data/4/.

REFERENCES

Baranes, H., S. L. Dykstra, D. A. Jay, and S. A. Talke, 2023: Sea level rise and variability in the Sacramento-San Joaquin Delta. *Sci. Rep.*, **13**, 22454, https://doi.org/10.1038/s41598-023-49204-z.

Buschman, F. A., A. J. F. Hoitink, M. van der Vegt, and P. Hoekstra, 2009: Subtidal water level variation controlled by river flow and tides. *Water Resour. Res.*, **45**, W10420, https://doi.org/10.1029/2009WR008167.

Cartwright, D. E., 1999: *Tides A Scientific History*. Cambridge University Press, 292 pp.

——, and A. C. Edden, 1973: Corrected tables of tidal harmonics. *Geophys. J. Int.*, **33**, 253–264, https://doi.org/10.1111/j.1365-246X.1973.tb03420.x.

Codiga, D. L., 2011: Unified tidal analysis and prediction using the UTide Matlab functions. GSO Tech. Rep. 2011-01, 60 pp., https://www.po.gso.uri.edu/~codiga/utide/2011Codiga-UTide-Report.pdf.

Consoli, S., D. Reforgiato Recupero, and V. Zavarella, 2014: A survey on tidal analysis and forecasting methods for Tsunami detection. *Sci. Tsunami Hazards J. Tsunami Soc. Int.*, **33**, 1–56.

Deser, C., A. S. Phillips, M. A. Alexander, and B. V. Smoliak, 2014: Projecting North American climate over the next 50 years: Uncertainty due to internal variability. *J. Climate*, **27**, 2271–2296, https://doi.org/10.1175/JCLI-D-13-00451.1.

Devlin, A. T., D. A. Jay, S. A. Talke, and E. Zaron, 2014: Can tidal perturbations associated with sea level variations in the Western Pacific Ocean be used to understand future effects of tidal evolution? *Ocean Dyn.*, **64**, 1093–1120, https://doi.org/10.1007/s10236-014-0741-6.

——, ——, ——, E. D. Zaron, and J. Pan, 2018: Seasonality of tides in Southeast Asian waters. *J. Phys. Oceanogr.*, **48**, 1169–1190, https://doi.org/10.1175/JPO-D-17-0119.1.

Downing-Kunz, M. A., P. A. Work, and D. H. Schoellhamer, 2021: Tidal asymmetry in ocean-boundary flux and in-estuary trapping of suspended sediment following watershed storms: San Francisco Estuary, California, USA. *Estuaries Coasts*, **44**, 2194–2211, https://doi.org/10.1007/s12237-021-00929-y.

Dykstra, S. L., Dzwonkowski, B., and Torres, R., 2022: The role of river discharge and geometric structure on diurnal tidal dynamics, Alabama, USA. *J. Geophys. Res. Oceans*, **127**, e2021JC018007, https://doi.org/10.1029/2021JC018007.

Familkhalili, R., S. A. Talke, and D. A. Jay, 2020: Tide-storm surge interactions in highly altered estuaries: How channel deepening increases surge vulnerability. *J. Geophys. Res. Oceans*, **125**, e2019JC015286, https://doi.org/10.1029/2019JC015286.

Fischer, N. I., 1993: *Statistical Analysis of Circular Data*. Cambridge University Press, 277 pp.

Flinchem, E. P., and D. A. Jay, 2000: An introduction to wavelet transform tidal analysis methods. *Estuarine Coastal Shelf Sci.*, **51**, 177–200, https://doi.org/10.1006/ecss.2000.0586.

Foreman, M. G. G., 1977: Manual for tidal heights analysis and prediction. Institute of Ocean Sciences Pacific Marine Science Rep. 77-10, 66 pp.

——, J. Y. Cherniawsky, and V. A. Ballantyne, 2009: Versatile harmonic tidal analysis: Improvements and applications. *J. Atmos. Oceanic Technol.*, **26**, 806–817, https://doi.org/10.1175/2008JTECHO615.1.

Gagniuc, P. A., 2017: *Markov Chains: From Theory to Implementation and Experimentation*. John Wiley and Sons, 256 pp.

Gan, M., H. Pan, Y. Chen, and S. Pan, 2021: Application of the Variational Mode Decomposition (VMD) method to river tides. *Estuarine Coastal Shelf Sci.*, **261**, 107570, https://doi.org/10.1016/j.ecss.2021.107570.

Godin, G., 1972: *The Analysis of Tides*. University of Toronto Press, 264 pp.

——, 1999: The propagation of tides up rivers with special considerations on the Upper Saint Lawrence River. *Estuarine Coastal Shelf Sci.*, **48**, 307–324, https://doi.org/10.1006/ecss.1998.0422.

Guo, L., M. van der Wegen, D. A. Jay, P. Matte, Z. B. Wang, D. Roelvink, and Q. He, 2015: River-tide dynamics: Exploration of nonstationary and nonlinear tidal behavior in the Yangtze River estuary. *J. Geophys. Res. Oceans*, **120**, 3499–3521, https://doi.org/10.1002/2014JC010491.

Haigh, I. D., and Coauthors, 2020: The tides they are a-changin': A comprehensive review of past and future nonastronomical changes in tides, their driving mechanisms, and future implications. *Ann. Rev. Geophys.*, **57**, e2018RG00636, https://doi.org/10.1029/2018RG000636.

Helaire, L. T., S. A. Talke, D. A. Jay, and D. Mahedy, 2019: Historical changes in Lower Columbia River and estuary floods: A numerical study. *J. Geophys. Res. Oceans*, **124**, 7926–7946, https://doi.org/10.1029/2019JC015055.

——, ——, ——, and H. Chang, 2020: Present and future flood hazard in the Lower Columbia River Estuary: Changing flood hazards in the Portland-Vancouver Metropolitan area. *J. Geophys. Res. Oceans*, **125**, e2019JC015928, https://doi.org/10.1029/2019JC015928.

Hoitink, A. J. F., and D. A. Jay, 2016: Tidal river dynamics: Implications for deltas. *Rev. Geophys.*, **54**, 240–272, https://doi.org/10.1002/2015RG000507.

Horsburgh, K. J., and C. Wilson, 2007: Tide-surge interaction and its role in the distribution of surge residuals in the North Sea. *J. Geophys. Res.*, **112**, C08003, https://doi.org/10.1029/2006JC004033.

Innocenti, S., P. Matte, V. Fortin, and N. Bernier, 2022: Analytical and residual bootstrap methods for parameter uncertainty assessment in tidal analysis with temporally correlated noise. *J. Atmos. Oceanic Technol.*, **39**, 1457–1481, https://doi.org/10.1175/JTECH-D-21-0060.1.

Jay, D. A., 1984: *Circulatory Processes in the Columbia River Estuary*. CREST, 169 pp.

——, 1997: Super-resolution of tides revisited. *Abstracts of "Ocean Interfaces", the Fifth Meeting of the Oceanography Society*, Seattle, WA. The Oceanography Society.

——, 2009: Evolution of tidal amplitudes in the Eastern Pacific Ocean. *Geophys. Res. Lett.*, **36**, L04603, https://doi.org/10.1029/2008GL036185.

——, and D. Smith, 1990: Circulation, density distribution and neap-spring transitions in the Columbia River Estuary. *Prog. Oceanogr.*, **25**, 81–112, https://doi.org/10.1016/0079-6611(90)90004-L.

——, and E. P. Flinchem, 1995: Wavelet transform analyses of non-stationary tidal currents. *Proc. IEEE Fifth Working Conf. on Current Measurement*, St. Petersburg, FL, Institute of Electrical and Electronics Engineers, 101–105, https://doi.org/10.1109/CCM.1995.516158.

——, and ——, 1997: Interaction of fluctuating river flow with a barotropic tide: A demonstration of wavelet tidal analysis methods. *J. Geophys. Res.*, **102**, 5705–5720, https://doi.org/10.1029/96JC00496.

——, and ——, 1999: A comparison of methods for analysis of tidal records containing multi-scale non-tidal background energy. *Cont. Shelf Res.*, **19**, 1695–1732, https://doi.org/10.1016/S0278-4343(99)00036-9.

——, and T. Kukulka, 2003: Revising the paradigm of tidal analysis – The uses of non-stationary data. *Ocean Dyn.*, **53**, 110–125, https://doi.org/10.1007/s10236-003-0042-y.

——, and P. K. Naik, 2011: Distinguishing human and climate influences on hydrological disturbance processes in the Columbia River, USA. *Hydrol. Sci. J.*, **56**, 1186–1209, https://doi.org/10.1080/02626667.2011.604324.

——, K. Leffler, and S. Degens, 2011: Long-term evolution of Columbia River tides. *J. Waterw. Port Coastal Ocean Eng.*, **137**, 182–191, https://doi.org/10.1061/(ASCE)WW.1943-5460.0000082.

——, ——, H. L. Diefenderfer, and A. B. Borde, 2014: Tidal-fluvial and estuarine processes in the Lower Columbia River: I. Along-channel water level variations, Pacific Ocean to Bonneville Dam. *Estuaries Coasts*, **38**, 415–433, https://doi.org/10.1007/s12237-014-9819-0.

——, A. B. Borde, and H. L. Diefenderfer, 2016: Tidal-fluvial and estuarine processes in the Lower Columbia River: II. Water

level models, floodplain wetland inundation, and system zones. *Estuaries Coasts*, **39**, 1299–1324, https://doi.org/10.1007/s12237-016-0082-4.

——, A. T. Devlin, D. Idier, E. W. Prokocki, and R. E. Flick, 2022: Tides and coastal geomorphology: The role of nonstationary processes. *Treatise Geomorphol.*, **8**, 161–198, https://doi.org/10.1016/B978-0-12-818234-5.00166-8.

Kaiser, G., 2011: *A Friendly Guide to Wavelets*. Birkhäuser, 300 pp.

Kay, D. J., and D. A. Jay, 2003: Interfacial mixing in a highly-stratified estuary 2. A "method of constrained differences" approach for the determination of the momentum and mass balances and the energy of mixing. *J. Geophys. Res.*, **108**, 3073, https://doi.org/10.1029/2000JC000253.

Kimmerer, W., and Coauthors, 2019: Effects of drought and the emergency drought barrier on the ecosystem of the California Delta. *San Francisco Estuary Watershed Sci.*, **17**, 2, https://doi.org/10.15447/sfews.2019v17iss3art2.

Knowles, N., 2002: Natural and management influences on freshwater inflows and salinity in the San Francisco Estuary at monthly to interannual scales. *Water Resour. Res.*, **38**, 1289, https://doi.org/10.1029/2001WR000360.

Kukulka, T., and D. A. Jay, 2003a: Impacts of Columbia River discharge on salmonid habitat: 1. A nonstationary fluvial tide model. *J. Geophys. Res.*, **108**, 3293, https://doi.org/10.1029/2002JC001382.

——, and ——, 2003b: Impacts of Columbia River discharge on salmonid habitat: 2. Changes in shallow-water habitat. *J. Geophys. Res.*, **108**, 3294, https://doi.org/10.1029/2003JC001829.

Leffler, K. E., and D. A. Jay, 2009: Enhancing tidal harmonic analysis: Robust (hybrid L^1/L^2) solutions. *Cont. Shelf Res.*, **29**, 78–88, https://doi.org/10.1016/j.csr.2008.04.011.

Li, S., T. Wahl, S. A. Talke, D. A. Jay, P. M. Orton, X. Liang, G. Wang, and L. Liu, 2021: Evolving tides aggravate nuisance flooding along the U.S. coastline. *Sci. Adv.*, **7**, eabe2412, https://doi.org/10.1126/sciadv.abe2412.

Matte, P., D. A. Jay, and E. D. Zaron, 2013: Adaptation of classical tidal harmonic analysis to nonstationary tides, with application to river tides. *J. Atmos. Oceanic Technol.*, **30**, 569–589, https://doi.org/10.1175/JTECH-D-12-00016.1.

Moftakhari, H., Muñoz, A. A. Asanjan, A. AghaKouchak, H. Moradkhani, and D. A. Jay, 2024: Nonlinear interactions of sea-level rise and storm tide alter extreme coastal water levels: How and why? *AGU Adv.*, **5**, e2023AV000996, https://doi.org/10.1029/2023AV000996.

Moftakhari, H. R., D. A. Jay, S. A. Talke, T. Kukulka, and P. D. Bromirski, 2013: A novel approach to flow estimation in tidal rivers. *Water Resour. Res.*, **49**, 4817–4832, https://doi.org/10.1002/wrcr.20363.

——, ——, ——, and D. H. Schoellhamer, 2015: Estimation of historic flows and sediment loads to San Francisco Bay, 1849–2011. *J. Hydrol.*, **529**, 1247–1261, https://doi.org/10.1016/j.jhydrol.2015.08.043.

——, ——, and ——, 2016: Estimating river discharge using multiple-tide gages distributed along a channel. *J. Geophys. Res. Oceans*, **121**, 2078–2097, https://doi.org/10.1002/2015JC010983.

Monismith, S. G., W. Kimmerer, J. R. Burau, and M. T. Stacey, 2002: Structure and flow-induced variability of the subtidal salinity field in northern San Francisco Bay. *J. Phys. Oceanogr.*, **32**, 3003–3019, https://doi.org/10.1175/1520-0485(2002)032<3003:SAFIVO>2.0.CO;2.

Munk, W. H., and K. Hasselmann, 1964: Super-resolution of tides. *Studies on Oceanography—A Collection of Papers Dedicated to Koji Hidaka*, K. Yoshida, Ed., University of Tokyo, 339–344.

——, and D. E. Cartwright, 1966: Tidal spectroscopy and prediction. *Philos. Trans. Roy. Soc.*, **A259**, 533–581, https://doi.org/10.1098/rsta.1966.0024.

Naik, P., and D. A. Jay, 2011: Human and climate impacts on Columbia River hydrology and salmonids. *River Res. Appl.*, **27**, 1270–1276, https://doi.org/10.1002/rra.1422.

Pan, H., and X. Lv, 2019: Reconstruction of spatially continuous water levels in the Columbia River estuary: The method of Empirical Orthogonal Function revisited. *Estuarine Coastal Shelf Sci.*, **222**, 81–90, https://doi.org/10.1016/j.ecss.2019.04.011.

——, Z. Guo, Y. Wang, and X. Lv, 2018a: Application of the EMD method to river tides. *J. Atmos. Oceanic Technol.*, **35**, 809–819, https://doi.org/10.1175/JTECH-D-17-0185.1.

——, X. Lv, Y. Wang, P. Matte, H. Chen, and G. Jin, 2018b: Exploration of tidal-fluvial interaction in the Columbia River Estuary using S_TIDE. *J. Geophys. Res. Oceans*, **123**, 6598–6619, https://doi.org/10.1029/2018JC014146.

——, T. Xu, and Z. Wei, 2023a: Anomalously large seasonal modulations of shallow water tides at Lamu, Kenya. *Estuarine Coastal Shelf Sci.*, **281**, 108203, https://doi.org/10.1016/j.ecss.2022.108203.

——, ——, and ——, 2023b: A modified tidal harmonic analysis model for short-term water level observations. *Ocean Model.*, **186**, 102251, https://doi.org/10.1016/j.ocemod.2023.102251.

Pawlowicz, R., B. Beardsley, and S. Lentz, 2002: Classical tidal harmonic analysis including error estimates in MATLAB using T_TIDE. *Comput. Geosci.*, **28**, 929–937, https://doi.org/10.1016/S0098-3004(02)00013-4.

Ray, R. D., 2006: Secular changes of the M2 tide in the Gulf of Maine. *Cont. Shelf Res.*, **26**, 422–427, https://doi.org/10.1016/j.csr.2005.12.005.

Reidy, M. S., 2008: *Tides of History Ocean Science and Her Majesty's Navy*. University of Chicago Press, 392 pp.

Rioul, O., and M. Vetterli, 1991: Wavelets and signal processing. *IEEE Signal Process. Mag.*, **8**, 14–38, https://doi.org/10.1109/79.91217.

Simon, B., 1991: The species concordance method of tide prediction. *Tidal Hydrodynamics*, B. B. Parker, Ed., John Wiley and Sons, 725–736.

Talke, S. A., and D. A. Jay, 2020: Changing tides: The role of natural and anthropogenic factors. *Annu. Rev. Mar. Sci.*, **12**, 121–151, https://doi.org/10.1146/annurev-marine-010419-010727.

——, A. Mahedy, D. A. Jay, P. Lau, C. Hilley, and A. Hudson, 2020: Sea level, tidal, and river flow trends in the Lower Columbia River Estuary, 1853–present. *J. Geophys. Res. Oceans*, **125**, e2019JC015656, https://doi.org/10.1029/2019JC015656.

Tilai, L., C. Liming, G. Xiangyu, and D. Lei, 2019: Analysis of sediment deposition downstream tidal sluice of estuary. *10th Int. Conf. on Asian Pacific Coasts*, Hanoi, Vietnam, Springer, 649–655, https://doi.org/10.1007/978-981-15-0291-0_89.

Zaron, E., and D. A. Jay, 2014: An analysis of secular change in tides at open-ocean sites in the Pacific. *J. Phys. Oceanogr.*, **44**, 1704–1726, https://doi.org/10.1175/JPO-D-13-0266.1.